Late Quaternary history of the Kerch Strait — the stratotype region for the Black Sea

Daria Semikolennykh [a,b,*]

[a] *School of Geography, Archaeology and Environmental Studies, University of the Witwatersrand, Private Bag 3, WITS, 2050, South Africa*
[b] *Institute of Geography, Russian Academy of Sciences, Staromonetny Lane 29, Moscow, 119017, Russia*

A B S T R A C T

The Kerch Strait has periodically connected to the Black, Azov, and Caspian seas throughout its Late Quaternary history. The strait's deposits reflect the changes in the natural environment of the entire Ponto-Caspian region, which are a response to global climate change. Several studies have been done on the region's stratigraphy, biostratigraphy, geomorphology, and paleogeography. However, most of the current knowledge about the paleogeography of the area is based on the analysis of empirical data collected more than 25 years ago, and due to the lack of detailed geochronological studies, many palaeogeographical problems remain unresolved.

This paper presents a reconstruction of environmental change in the Kerch Strait during the Late Quaternary. The reconstruction is based on the results of a comprehensive study of the sedimentary sequences in the Kerch Strait carried out by the author and colleagues over the past ten years. The study examines the deposits of two stratotype sections of the Karangatian (Eemian) transgression and the four boreholes' sections in Tuzla Island in the central part of the strait.

A biostratigraphic division of the Upper Quaternary deposits of the Kerch Strait was carried out based on a malacofaunal study. Mollusc assemblages corresponding to various paleogeographic stages of development were identified, and their paleoecological characteristics were described. Luminescence and radiocarbon ages made it possible to determine the time intervals of established paleogeographic stages in the strait's history. Detailed luminescence dating of the Karangatian transgression sediments of the Eltigen and Tuzla stratotype sections has been carried out for the first time.

Six main stages in the Kerch Strait natural environment development were established in the Late Quaternary and correlated with global and regional climatic events: Karangatian, with three stages (MIS 5e-c); Tarkhankutian (MIS 5a); Post-Karangatian (MIS 4); Surozh (MIS 3); Neoeuxinian, with two stages (MIS 2); and Chernomorian (MIS 1). Two episodes of the Caspian waters flowing through the Kerch Strait into the Black Sea were identified in MIS 5c and at the end of MIS 2.

1. Introduction

The Kerch Strait is an essential link in the Mediterranean—Pont—Caspian system. During the Late Quaternary period, the strait served as a passage for Mediterranean marine waters into the Sea of Azov and the Manych Depression and for the flow of brackish Caspian waters into the Black and Mediterranean seas (Badertscher et al., 2011; Tudryn et al., 2016; Krijgsman et al., 2019; Yanina, 2020). Hence, studying the Quaternary deposits of the Kerch Strait allows us to reconstruct the connections between the Mediterranean, Black, Azov, and Caspian seas. It also enables tracing the development of the natural environment of the entire basin system, which is closely linked to global climate changes (Yanina, 2014; Krijgsman et al., 2019; Hoyle et al., 2021; Erginal et al., 2022). In the Quaternary sediments of the strait, there are deposits containing various mollusc assemblages representing different stages of the Kerch Strait area and the surrounding region's development. Mollusc assemblages in the Kerch Strait consist primarily of migratory rather than evolutionary species (Yanina et al., 2024) and show the alternation of the marine Mediterranean, brackish Caspian, and freshwater fauna (Nevesskaya, 1965).

Andrusov (1918) was first to describe the stratigraphy of the Kerch Strait's successions in up to 47.5 m deep 28 boreholes. He

identified four chronostratigraphic units, namely Chaudinian, Euxinian, Tyrrhenian (Karangatian), and modern, which host faunal complexes of the same name. The comprehensive studies of the Kerch Strait sediments were continued by Pravoslavlev (1928), Eberzin (1935), Arkhangelsky and Strakhov (1938) and many others (see review in Yanina, 2020). Fundamental interdisciplinary monographs, which have remained relevant, were written by Fedorov (1963, 1978), Shnyukov et al. (1981), and Popov (1983). The fauna in the sediments was studied by Nevesskaya (1965), Yanko et al. (1990), Chepalyga (2006), etc. Attempts have been made to date the sediments by U/Th (Arslanov et al., 1972), radiocarbon (Semenenko and Kovaluykh, 1973; Zubakov, 1974; Arslanov et al., 1983), thermoluminescence (Zubakov, 1988), paleomagnetic (Pilipenko and Trubikhin, 2012, 2015) and other methods.

However, there is still no consensus regarding the chronology of events in the Kerch Strait, their characteristics, and their relationship with regional and global climate changes, mainly due to the absence of reliable geochronological data. This article summarises a decade of research by the author and colleagues in the Kerch Strait. It presents a detailed overview of the sedimentary deposits from the Late Quaternary period found in the strait's coastal outcrops and boreholes. New stratigraphic, biostratigraphic, and geochronological data were collected and analysed to comprehensively understand the strait's palaeogeographic history. For the first time in the region, OSL dating of two stratotype sections — the Eltigen and the Tuzla — was carried out. The main aim of the research is to reconstruct the palaeogeographic events in the Kerch Strait over the last 130,000 years (MIS 5e—MIS 1), which has the potential to improve understanding of the paleogeography of the entire region. This period encompasses a range of significant global climatic events, including interglacial (Eemian/Mikulino) and glacial (Weichselian/Valdai) periods.

2. Background

2.1. Regional setting and stratigraphy

The Kerch Strait and the adjacent Kerch and Taman peninsulas (Fig. 1a and b) are structurally mainly located within the Kerch-Taman periclinal trough belonging to the Alpine mobile folding belt (Khain and Popkov, 2009). The formation of the Kerch-Taman trough as a tectonic element began at the turn of the late Eocene — early Oligocene in connection with the beginning of the formation of the folded mountain structure of the Greater Caucasus (Afanasenkov et al., 2007). The trough is characterised by the development of anticlines of a sub-latitudinal strike, expressed in the relief of the Kerch and Taman peninsulas by hills with a relative height of up to 100 m (Baskakova and Nikishin, 2018), which continue into the waters of the Kerch Strait (Shnyukov et al., 1986) (Fig. 1b).

The Kerch Strait is a shallow, unstratified strait in which water exchange occurs alternately from one sea to another (Mikhailov et al., 2010). Geologically, the Kerch Strait has a cross-cutting character (Shnyukov et al., 1981). The reason for its spatial localisation is that it is a tectonically weakened zone, emphasised by the activity of the paleo-Don River, the mouth of which extended into the Black Sea during glaciations. Thus, the strait has both tectonic and erosional origins. In

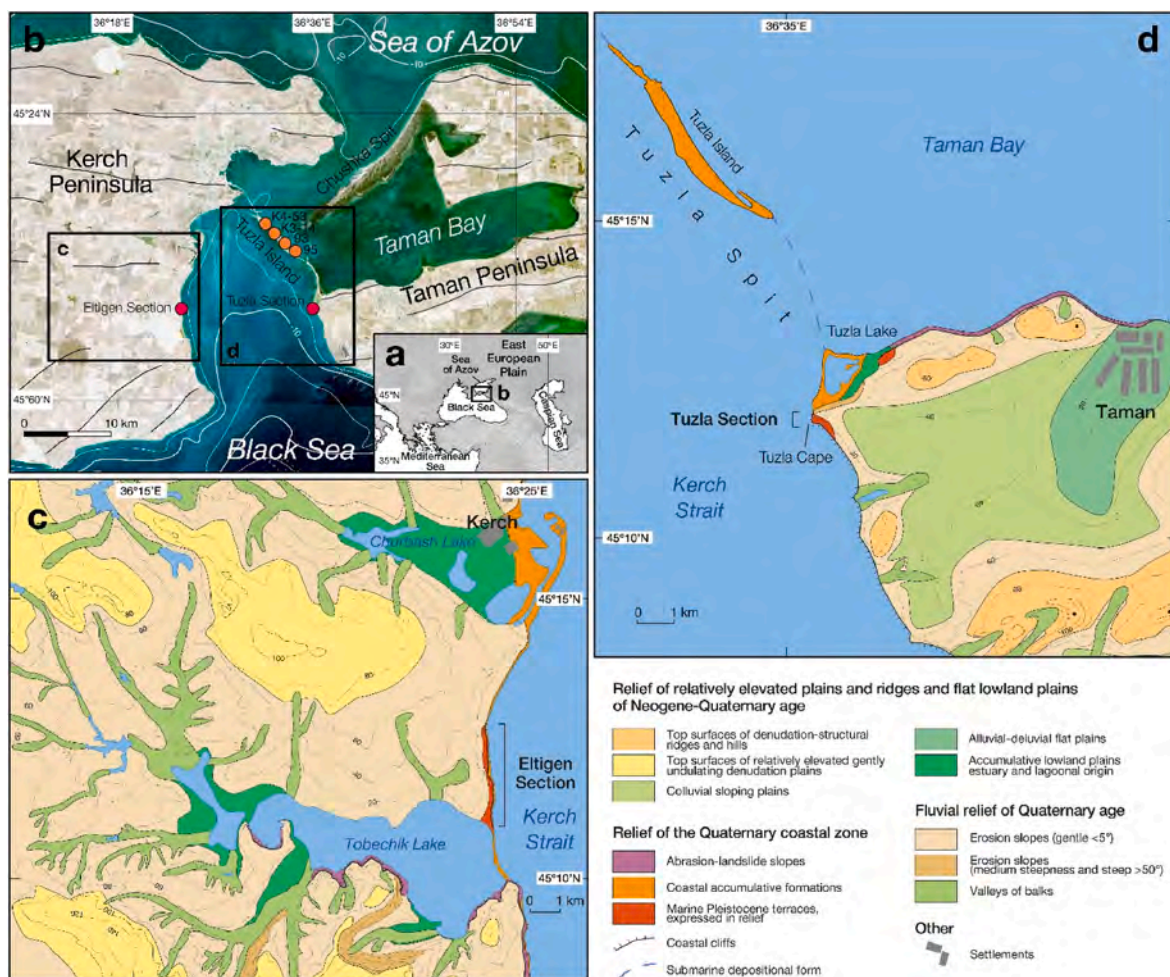Fig. 1. Location of the Kerch Strait (a) the studied sites (b). The lines in Fig. 1b show the axes of an anticline according to Trikhunkov et al. (2019). The geomorphological scheme and location of the (c) Eltigen and (d) Tuzla sections are shown according to Blagovolin (1962).

the lower pre-Oligocene structural levels, deep and regional faults are visible, which determined the configuration and emergence of the Kerch Strait (Shnyukov et al., 1981).

The Kerch Strait has a complex geomorphological structure: asymmetrical cross profile with the deepest part in the west, extended accumulative forms in the east (e.g. Tuzla Island, Chushka Spit), large bays (Taman Bay, Dinskaya Bay, Kerch and Kamysh-Burun Bays) (Ignatov and Chistov, 2003). The maximum depth of the Kerch Strait in the middle part is 8–9 m. The widest part of the strait is in its southern part and reaches 22 km with a depth of up to 19 m. The natural narrowest part is between Pavlovsky Cape and the northern end of the Tuzla Spit, which is 3.5 km. The bottom sediments of the strait are varied in lithological and granulometric composition: sands make up Tuzla Island, Chushka Spit, and individual shallows, and in the deeper parts of the strait, bottom sediments are represented by fine silty and silty-clayey silts. The shores of the strait are composed of easily eroded rocks that are susceptible to active exogenous geomorphological processes: coastal abrasion and landslides (Bagriy et al., 2008).

The thickness of the Quaternary marine sediments is small: in the north and south of the strait, the thickness of the sedimentary cover does not exceed 20–30 m; the central part is filled with recent sediments with a thickness of 50 m or more (Shnyukov et al., 1981).

The Kerch Strait has three main stratigraphic units of the Late Pleistocene age (Yanina, 2012): Karangatian, Neoeuxinian, and Chernomorian (Black Sea) sediments.

Deposits of the Karangatian age are exposed in scattered outcrops along the shores of the Kerch Strait in the form of relatively thick accumulative terraces and the coastal areas of the strait. There is no evidence in the Kerch-Taman region of Karangatian sediments filling any ancient erosional forms and penetrating inland (Blagovolin, 1960). Marine Karangatian sediments quickly thin out at a distance from the sea and are replaced along strike by continental loams. In the central part of the Kerch Strait, the Karangatian Basin was partially drained at the initial stage. There is a gradual transition from Euxinian (MIS 6) to Karangatian (MIS 5) sediments (Shnyukov et al., 1981). The maximum thickness of sediments of Karangatian age at the Kerch Strait bottom reached 19 m.

In the post-Karangatian time, erosion of the Pleistocene sediments previously deposited here occurred in the Kerch Strait. Neoeuxinian deposits overlap transgressively on Neogene, Euxinian, Karangatian, and post-Karangatian deposits at depths −68 to −11 m (Shnyukov et al., 1981). The shores of the strait are covered mainly by loess-soil and alluvium deposits in the deepened gullies (up to 10 m below modern sea level) since intense erosion occurred during this period, coinciding with a rapid drop in sea level (Blagovolin, 1960). Above the Neoeuxinian sediments lie the Chernomorian (Black Sea) sediments, marking the beginning of the Holocene transgression.

2.2. Previous studies

The crucial sections of Upper Pleistocene deposits within the Kerch Strait are the Eltigen (Kerch Peninsula) and the Tuzla (Taman Peninsula) (Fig. 1c and d). Due to their central position in the strait's outlines, the Upper Quaternary sediments of the Kerch Strait bed around the Tuzla Spit (Fig. 1d) represent the most complete Late Pleistocene and Holocene sequences.

2.2.1. Eltigen section

The Eltigen section is a stratotype of the transgressive Karangatian sediments from the MIS 5. This section is exposed in coastal outcrops in the Azov-Black Sea region (Andrusov, 1904). Most paleogeographical conclusions about the Karangatian Basin's paleogeography are based on analyses of the Eltigen section.

The section is situated in a coastal outcrop on the western coast of the Kerch Strait, between the village of Geroevskoye and the embankment that separates Lake Tobechik from the sea (Fig. 1c). It spans a length of

approximately 3.5 km. From a geological and tectonic perspective, the Eltigen section is located on the flank of an anticline (Fig. 1b and c) (Blagovolin, 1962). This fold is still deforming, as seen in the displacement of marine sediments with a Karangatian fauna (Blagovolin, 1962; Fedorov, 1963). The presence of Paleogene clays in the middle part of the section indicates recent tectonic movements. The area to the south of the section, occupied by Lake Tobechik, is presently experiencing submersion (Simonov and Bryantseva, 2018).

Numerous researchers, including Dodonov et al. (2000), Shelkoplyas and Khristoforova (2007), Svitoch (2009) and others, have studied the deposits of the section. However, there is still no consensus on the correlation between the deposits in the section, the number of phases of the Karangatian transgression and their age.

Several authors (see, for example, Nevesskaya, 1965; Zubakov, 1988; Yanko et al., 1990; Shelkoplyas and Khristoforova, 2007) have expressed the opinion that the southern part of the Eltigen section contains deposits from the first (estuary) phase of the Karangatian transgression. These deposits consist of a layered mixture of clays, silts, and sands, along with a euryhaline molluscan fauna. Meanwhile, the sediments from the phase of maximum development of the transgression, found in the central and northern parts of the section, consist of various sand, gritstone, and coquina, with the inclusion of a stenohaline molluscan fauna. Fedorov (1978) criticised the idea that the estuary sediments found in the Eltigen section were deposits from the first phase of the Karangatian transgression. He argued that the facies' variability alone was insufficient evidence to support this claim.

Based on the analysis of molluscan fauna in the Eltigen sediments, most researchers (Fedorov, 1978; Yanko et al., 1990; Chepalyga, 2002; Svitoch, 2009; Yanina, 2012; etc.) suggest 2–3 phases (still debatable) of the Karangatian transgression. The initial and/or final phases are characterised by mollusc complexes similar to those living in the modern Black Sea. However, sediments of one of the Karangatian transgression phases include the most thermophilic and halophytic Mediterranean species of molluscs, which are absent in the modern Black Sea. Such indicator species of the maximum phase of transgression include *Paphia senescens*, *Mytilus galloprovincialis*, *Flexopecten glaber*, and *Acanthocardia tuberculata* primarily (Nevesskaya, 1965; Fedorov, 1978; Shnyukov et al., 1981; Yanina, 2012).

Additionally, one hypothesis suggests that the sediment unit at the top of the section marks the start of the fourth phase of the Karangatian transgression development. During this phase, the malacofaunal composition was depleted (Nevesskaya, 1965), and certain species of foraminifera, which are absent in the modern-day Black Sea, disappeared (Yanko et al., 1990).

The first absolute dates were obtained for the Eltigen section deposits by Arslanov et al. (1972) using the U/Th method. The results showed that the age of the deposits fell in the range of 88.3–81.6 ka BP. Additionally, radiocarbon dating was used to determine the age of the marine sediments in the section. Semenenko and Kovaluykh (1973) and Zubakov (1974) found that the age of the deposits ranged from 42 to 27 ka BP. Due to the physical limitations of the radiocarbon method, dating data cannot be considered reliable. Later, the deposits were again dated by the U/Th method; all results were 127–58 ka BP (Arslanov et al., 1983; Dodonov et al., 2000). An attempt was made to determine the age of the deposits of the first (Tobechik) transgression phase using the TL method. The dating result showed that the top of the formation is 205.0 ± 50.0 ka BP (Zubakov, 1988).

Various geochronological methods were employed to determine the age of sediments in the Eltigen section, which was correlated with MIS 5. However, more accurate time intervals still need to be established. Additionally, there is still a lack of understanding regarding the relationship between different facies layers within the section.

2.2.2. Tuzla section

The Tuzla section is a stratotype of the Karangatian transgression sediments (MIS 5), located on the western coast of the Taman Peninsula

at the base of the spit of the same name near the axis of an anticline (Rogozhin et al., 2015) (Fig. 1b–d). The description of pre-Quaternary and Quaternary sediments here was carried out by Andrusov (1903), Pravoslavlev (1928), and Eberzin (1935). Subsequently, the section was studied many times by Fedorov (1963), Shnyukov et al. (1981), Zubakov (1988), Svitoch and Novichkova (2001), Pilipenko et al. (2007), Svitoch (2009), Pilipenko and Trubikhin (2012) and others. The Karangatian deposits in the Tuzla section are only a few meters thick and have a less diverse faunal complex than the Eltigen section. These deposits most likely represent a single phase of the transgression (Svitoch, 2009).

The upper Quaternary deposits of the section were dated for the first time by Arslanov et al. (1972). They used the U/Th method and took a mollusc shell's inner and outer layers from a 0.5–0.8 m depth from the top of marine sediments with the Karangatian fauna. The result showed that the deposits were 33.1 ± 2.8 and 37.7 ± 3.3 ka BP. Later, an attempt was made to determine the age of the deposits using the radiocarbon method (Zubakov, 1974). However, the date turned out to be beyond the limits of the method (i.e. older than 40.2 ka BP). Thirty years later, Pilipenko and Trubikhin (2012), using the paleomagnetic method, established the range of accumulation of Karangatian deposits to be 110–105 ka at a depth of 9.3–9.6 m in the section. At the Technical University of Denmark, they obtained the only OSL date of 85 ± 6 ka on sediments from the upper part of the marine strata (Pilipenko and Trubikhin, 2012). Hence, insufficient geochronological data in the Tuzla section prevents the chronology of sedimentary history from being established.

2.2.3. Tuzla Spit

The Tuzla Spit, which includes Tuzla Island, is a shelly sand accumulation, elongated in a northwest direction along the line Cape Tuzla — Cape Ak-Burun, originating on the coast of the Taman Peninsula (Fig. 1b–d). The total length of the spit, along with islands and underwater shoals, is approximately 12 km. Tuzla Island is approximately 8 km long, with a width that rarely exceeds 100 m, reaching 500 m only in its central part (Peshkov et al., 2005). Most sediment on the spit came from the erosion of Quaternary terraces between Cape Tuzla and Panagia. There was also some contribution from Taman Bay, but it was relatively minor. Material of biogenic origins, in particular mollusc shells, played a significant role in providing sediments to the spit.

According to Peshkov et al. (2005), the Tuzla Spit's modern body is a young formation that originated at a sea level 1.5–2.0 m lower than the present one, around 1.0–1.3 ka BP. However, the outline of the Tuzla Spit has changed multiple times since its formation (Pasynkov, 2005), sometimes creating a single entity or breaking into a system of islands. Its formation was mainly caused by the rise in sea level during the Holocene period. Additionally, clastic material from one of the branches of the Kuban delta was introduced into Taman Bay during the Neochernomorian (New Black Sea) period, which further contributed to the formation of the spit (Shnyukov et al., 1981). After the Kuban's flow changed direction, Tuzla stopped receiving terrigenous material and lost its role as a spit, and now it is a relict depositional form. The base of Tuzla Island is located at levels of −11 to −13 m and lies on a relatively flat surface of compacted marine silt (Peshkov et al., 2005).

The study of new factual material will clarify the stages of the Tuzla Spit formation and correlate local paleogeographical events in the central part of the Kerch Strait with regional events of the Ponto-Caspian system.

3. Material and methods

The study involved detailed lithological descriptions, malacofaunal and geochronological (OSL and radiocarbon dating) analysis. In total, 86 samples of malacofauna were studied, and 39 absolute dates were obtained.

Lithological analysis of sediments implied a field description of sections and borehole cores following Lowe and Walker (2015).

Particular attention was paid to the search and description of the bivalve molluscan fauna inclusions, which are decisive for stratigraphic constructions and paleogeographic reconstructions of the Quaternary history of the Ponto-Caspian Sea. Indicator species that make up specific malacofaunal complexes depending on environmental conditions were used to obtain paleogeographic information. This approach is widely used in the Ponto-Caspian region (Nevesskaya, 1965; Svitoch et al., 1999; Yanina, 2012) to dissect the sequence of Pleistocene and Holocene marine and lacustrine sediments.

The preparation of malacofaunal samples and their systematic analysis were performed at the Laboratory of Pleistocene Paleogeography (Lomonosov Moscow State University). Species identification was conducted using the Black and Caspian seas key mollusc species (Nevesskaya, 1965, 2007; Yanina, 2005, 2012) and reference collections. The identification of features and patterns of spatiotemporal distribution of malacofaunal communities in sections of recent sediments and borehole cores and their comparative analysis provided a biostratigraphic basis for the division of the Upper Pleistocene sedimentary sequence for establishing stages in the history of the functioning of the Kerch Strait and their paleoecological characteristics.

The ^{14}C dates were obtained by liquid scintillation counting methods (LSC) at the Laboratory of Paleogeography and Geochronology (St. Petersburg State University) and reported in Semikolennykh et al. (2018). The conventional ^{14}C ages were calibrated (2-sigma standard deviation) using the OxCal 4.4 program (Bronk Ramsey and Lee, 2013) with the IntCal20 calibration data set (Reimer et al., 2020). The paper presents conventional ^{14}C (BP) and calibrated ages (cal BP). No corrections were made for the δ^{13}C value and reservoir effect for samples belonging to the period of renewed connection between the Black and Mediterranean seas (younger than ∼8 ka), as these two effects are comparable in magnitude and make opposite contributions (Siani et al., 2016; Berndt et al., 2019). However, it is difficult to assess the significance of the reservoir effect for the period of the Black Sea isolation from the World Ocean, i.e. its value varies; in particular, in the interval 15–8 ka, it has a range of 900–1450 yr (Kwiecien et al., 2008). In this regard, the dating of 10.06 ± 0.34 cal ka BP (Table 4), obtained from the shell of a freshwater mollusc, is highly likely to be 500–1000 yr older. Due to the fact that it is impossible to accurately estimate the value of the reservoir age, the author believes that this dating gives reason to consider that the sediment approximately accumulated at the boundary of the Late Pleistocene and Holocene.

Luminescence measurements were performed at the Nordic Laboratory for Luminescence Dating (Aarhus University and Technical University of Denmark). Initial sample preparation was conducted at the Laboratory of Pleistocene Paleogeography (Lomonosov Moscow State University). Dating results are reported by Kurbanov et al. (2019, 2020) and Semikolennykh et al. (2023a).

Samples were collected at night in light-proof bags to prevent exposure to light; separately, selected material for gamma spectrometric analysis was collected. Sample preparation was carried out according to Murray et al. (2021). The single aliquot regeneration (SAR) dose protocol (Murray and Wintle, 2000, 2003) was used to determine the equivalent dose (De). Luminescence dating was carried out on 180–250 μm size quartz (18–24 aliquots) and feldspar (6–11 aliquots) grains. Luminescence measurements were performed on an automated Risø TL/OSL reader model DA-20 (Bøtter-Jensen et al., 2000, 2002). To construct a dose-response curve and determine the equivalent dose (De), grains were irradiated with the in-built ^{90}Sr/^{90}Y beta source, with the calibration doses recalculated following Autzen et al. (2022). For all samples, measurements were performed using three protocols (OSL, IR$_{50}$, and pIRIR$_{290}$). Feldspar can accumulate more luminescence signal than quartz, so for those sediments where quartz had reached the limit of dating capabilities, the chronology is based on the results obtained from the pIRIR$_{290}$ dating protocol for feldspars (Buylaert et al., 2012).

Radioactivity concentrations were measured using high-resolution gamma spectroscopy (Murray et al., 1987, 2018). The average gamma

and beta dose rates to the sediment were calculated using the conversion factors of Cresswell et al. (2018). The estimated gamma dose rate is adjusted for attenuation by soil moisture using a coefficient of 1.14 (Zimmerman, 1971). Beta attenuation due to grain size and water content follows Cunningham et al. (2022), accounting for the presence of U- and Th-series nuclides on grain surfaces. Dose rates to feldspars take account of an assumed internal K concentration. The contribution from cosmic radiation was estimated for each sample as a function of depth following Prescott and Hutton (1994).

The alternating layers of sand and silt in the Eltigen's outcrop A sediments posed challenges in dating. Results for three protocols were obtained only for four samples from seventeen, and they were in good agreement, i.e. the quartz is well-bleached. It was assumed that the sedimentation conditions of loess-like loams and sandy strata in outcrops A and B were identical and had the same origin. Since the dating of outcrop B showed reliable results (Kurbanov et al., 2019), the author believes that the dates obtained for outcrop A for sand strata are likely to be well-bleached and reliable (Fig. 2). Therefore, as the dates obtained for silty deposits do not contradict stratigraphically, there is reason to use these results for further paleogeographic reconstructions.

Similar to the Eltigen section's outcrop A, only one date of the Tuzla section (Kurbanov et al., 2020) corresponds with the three protocols (Fig. 3). However, assuming similar depositional conditions of the Karangatian sediments on the western and eastern shores of the Kerch Strait, the dating results are believed to be reliable.

4. Results

4.1. Eltigen section

The Eltigen section (Fig. 4a) is an abrasion ledge of a marine Pleistocene terrace with a 13–15 m height. The section reveals a sequence of predominantly coastal-marine sediments of the Karangatian transgression overlain by loess-like loams with two or three poorly developed paleosols.

The section was studied in its southern (N45°10′53.75 E36°24′17.45) and central (N45°11′04.92 E36°24′18.01) parts, which were designated as A and B, respectively. The section's central part (B) is located near the axis of the anticline, while the southern part (A) is closer to the Lake Tobechik's syncline.

5.8 m-high Eltigen section A includes the following units (Semikolennykh et al., 2023a): (1) light brown loam (modern chestnut soil) (Fig. 4b, interval 0.00–0.45 m) with plant roots, carbonate nodules, and shells of terrestrial molluscs; (2) pale loess-like loam (0.45–0.80 m) with plant roots, carbonate nodules and rare shells of terrestrial molluscs; (3) sandy pale loam (0.80–1.00 m) with pebbles, gravel and

redeposited shells of marine molluscs; (4) sandy pale loess-like loam (1.00–2.25 m) with rare shells of terrestrial molluscs; (5) obliquely and horizontally layered ferruginous pale sand (2.25–2.85 m) crushed into sedimentary folds with gravel and marine mollusc fauna; (6) bluish sandy clays (2.85–3.30 m) with rare small thin-valve shells of marine molluscs; (7) obliquely and horizontally layered ferruginous pale sand (3.30–3.55 m) with gravel and shells of marine molluscs; (8) light grey horizontally layered sandy clays (3.55–3.90 m) with small thin-valve shells of marine molluscs; (9) obliquely and horizontally layered ferruginous pale sand (3.90–4.30 m) with shells of marine molluscs, and gravel layer at the base; (10) light grey horizontally layered clays (4.30–4.50 m) with small thin-valve shells of marine molluscs; (11) dark grey clay with traces of ferrugination, apparent unit thickness 0.5 m.

At the Eltigen section's outcrop B, 13.0 m high, the following deposits are exposed (Kurbanov et al., 2019): (1) pale-brown loam (modern soil) (Fig. 4c, interval 0.0–1.5 m) with plant roots, carbonate nodules, gypsum druses and shells of terrestrial molluscs; (2, 4, 6) pale loess-like loam (1.5–5.5 m) with two paleosols (3, 5); (7) obliquely and horizontally layered pale sand (5.5–6.2 m) with shell detritus; (8) obliquely and horizontally layered light brown sand (6.2–9.0 m) with abundant molluscs shells, individual layers extremely rich in molluscs shells stand out; (9) obliquely and horizontally layered light brown compacted sand with an apparent thickness of 4.0 m with abundant mollusc shells and gravel.

The results of the malacofaunal analysis of deposits from the Eltigen section outcrops A and B are presented in Figs. 5 and 6. A complete list of species that make up the outcrops' malacofaunal complexes and their ecological preferences are presented in Supplementary Table 1.

At the outcrop A (Semikolennykh et al., 2023a), within the silty unit 10, a malacofaunal complex containing only two euryhaline mollusc species (*Cerastoderma glaucum* and *Abra segmentum*) in large quantities is identified. The euryhaline *Mytilaster lineatus* appears in the faunal complex in single quantities in sandy unit 9 up to 3.90 m. At a depth of 3.55–3.90 m in the silty unit 8, a depleted complex is represented by poorly developed and rare *Cerastoderma glaucum* and *Donax venustus*. In the interval of 3.30–3.55 m in the sandy unit 7, the number of shells and species diversity noticeably increases: along with *Cerastoderma glaucum*, *Abra segmentum* and *Mytilaster lineatus*, the complex is represented by *Parvicardium exiguum* and *Paphia senescens*. From a depth of 3.30 m (units 6, 5), the sediments contain moderately euryhaline molluscs, typical of the Karangatian transgression upper phase sediments: *Ostrea edulis* and *Chamelea gallina* (predominant), and euryhaline species.

At the Eltigen section's outcrop B (Kurbanov et al., 2019), in the interval 11.2–12.0 m (unit 9), the species composition of the malacofauna is dominated by moderately euryhaline species with *Ostrea edulis* prevailing. At a depth of 9.0–11.2 m (unit 9), stenohaline species
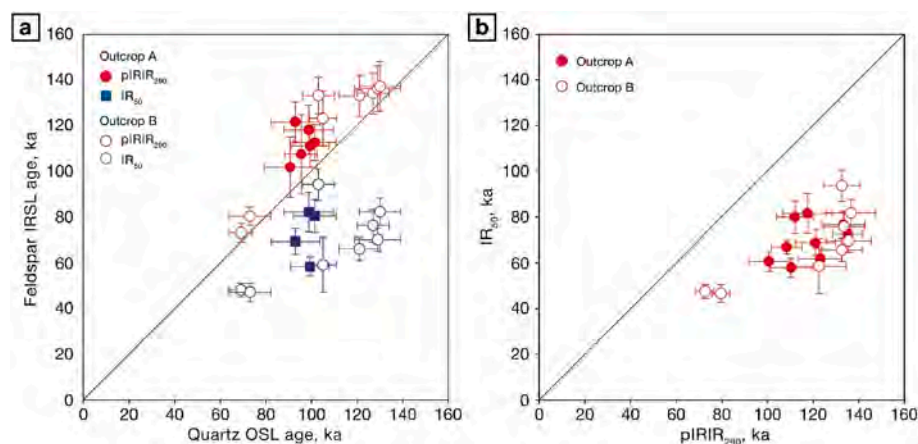

Fig. 2. Reliability of dating results for the Eltigen section's outcrop A: (a) comparison of results using OSL and IRSL protocols; (b) comparison of results using IRSL protocols.
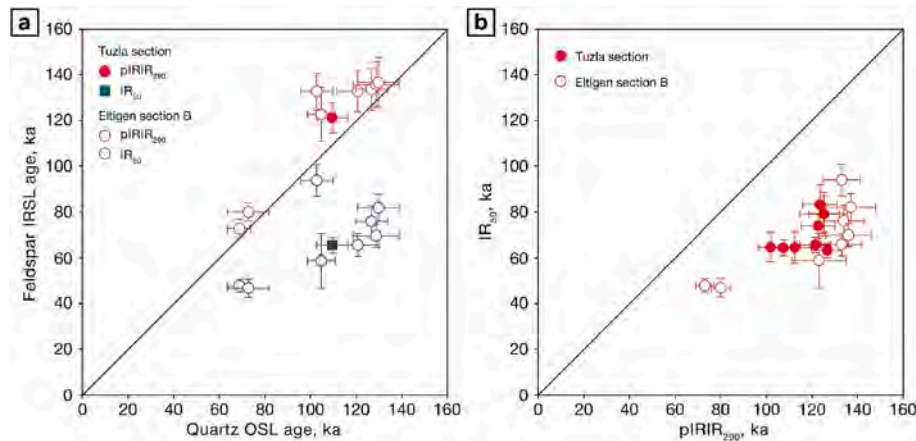
Fig. 3. Reliability of dating results for the Tuzla section: (a) comparison of results using OSL and IRSL protocols; (b) comparison of results using IRSL protocols.
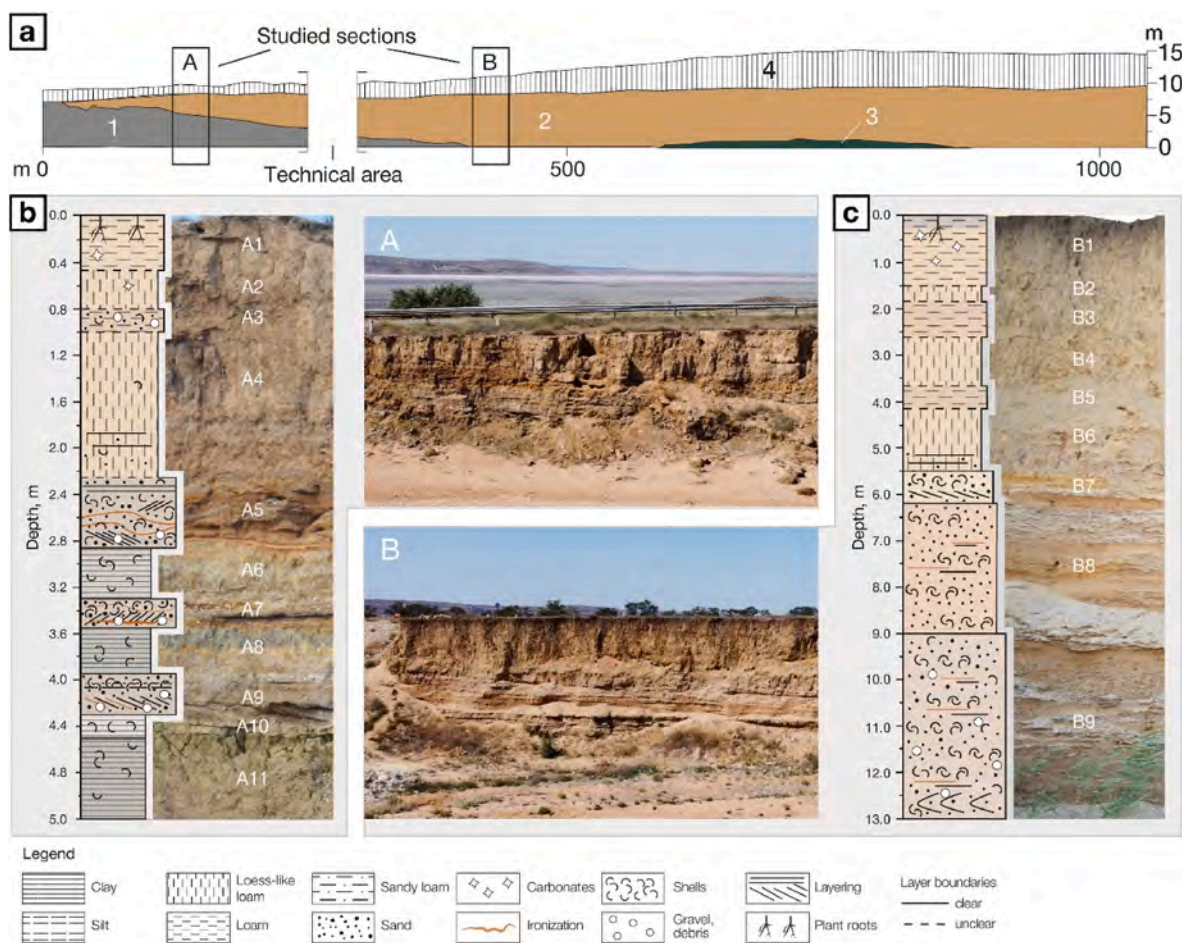

Fig. 4. Eltigen Section: (a) general scheme of the section (Dodonov et al., 2000): *1 — facies variable thickness of alternating sands and clays; 2 — coastal-marine sandy deposits; 3 — Sarmatian clays (Neogene); 4 — loess-soil formation;* (b) outcrop A; (c) outcrop B.

appear; the complex is dominated by *Ostrea edulis, Flexopecten glaber, Chlamelea gallina,* and *Abra segmentum.* The most remarkable species diversity of marine molluscs is represented in the range of 6.2–9.0 m (unit 8); the complex includes *Cerastoderma glaucum, Paphia senescens, Spisula subtruncata, Mytilus galloprovincialis,* there are rare shells of *Acanthocardia tuberculata* — the most halophytic species in the Kar-angatian faunal complex, which preferred salinity higher than 28‰ (Nevesskaya, 1965). At a depth of 5.5–6.2 m (unit 7) the composition of the faunal community is represented by euryhaline and moderately

euryhaline species; shell fragments predominate in the samples.

The results of luminescence dating of the Eltigen section's outcrops A and B are shown in Fig. 5 and are summarised in Tables 1 and 2, respectively. The outcrop B was dated first in 2017 (Kurbanov et al., 2019). Eight dates were obtained for the outcrop, two for loess-like loams (units 4, 6), and six for sea sands (units 7–9). The dating results from the three protocols (OSL, IR_{50} and $pIRIR_{290}$) show good agreement, indicating that the quartz was well-bleached before burial. The age of loess-like loams with paleosol ranges from 69 ± 5 to 73 ± 9 ka (Table 2,
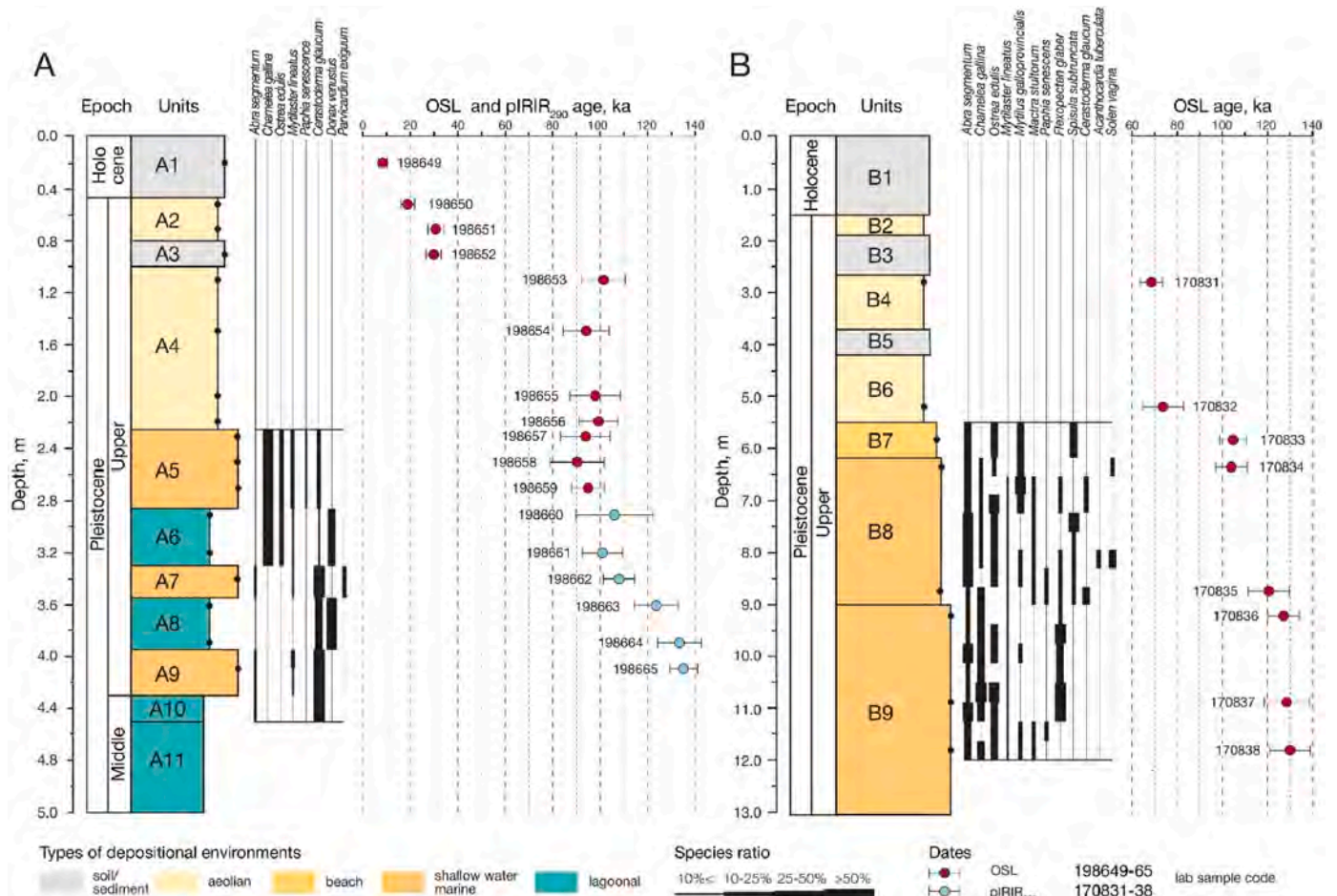
Fig. 5. Outcrop diagrams A and B of the Eltigen section with the results of malacofaunal and geochronological analyses.
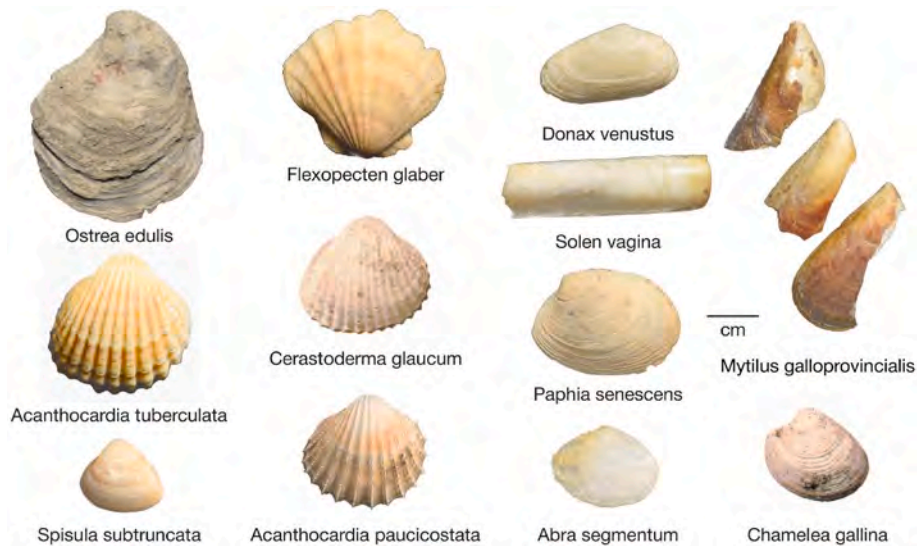
Fig. 6. Species found in the Eltigen and the Tuzla sections.

Fig. 5). The deposits of unit 7 are transitional from marine to continental, and their accumulation rate is relatively fast, and age is 105 ± 6 ka BP (Table 2, Fig. 5). The age of units 8 and 9, represented by typical coastal-marine sands with numerous mollusc fauna and separated by an erosional break, is estimated at 103 ± 7–121 ± 9 and 127 ± 7–130 ± 9 ka, respectively (Table 2, Fig. 5).

Sediments exposed in outcrop A have been dated in 2020–2021 (Semikolennykh et al., 2023a). The alternating layers of sand and silt in the outcrop sediments posed challenges in dating. A total of seventeen dates were obtained for the outcrop: eight dates for continental sediments (units 1–4), represented by loess-like loams, sandy loam and modern soil; six dates for marine sands (units 5, 7, 9), and four dates for

Table 1
Summary of luminescence data for the Eltigen section's outcrop A.

No	Sample code	Depth, cm	Unit	Lithology	WC, %	^{226}Ra, Bq kg^{-1}	^{232}Th, Bq kg^{-1}	^{40}K, Bq kg^{-1}	Dose rate, Bq ka^{-1} Quartz D_r, Bq ka^{-1}	Feldspar D_r, Bq ka^{-1}	IR$_{50}$ De, Gy	n	pIRIR$_{290}$ De, Gy	n	OSL De, Gy	n	IR$_{50}$ age, ka	pIRIR$_{290}$ age, ka	OSL age, ka
1	198649	20	1	Loam	10	32.1 ± 0.6	21.5 ± 0.5	198 ± 8	1.67 ± 0.07	2.60 ± 0.12	–	–	–	–	15.2 ± 0.9	14	–	–	**9.1 ± 0.7**
2	198650	50	2	Loess-like loam	10	32.0 ± 0.4	15.8 ± 0.3	115 ± 4	1.30 ± 0.06	2.24 ± 0.11	–	–	–	–	25.5 ± 3.3	22	–	–	**19.6 ± 2.9**
3	198651	70			10	28.7 ± 0.7	10.4 ± 0.5	53 ± 7	0.97 ± 0.05	1.91 ± 0.10	–	–	–	–	30.6 ± 2.7	21	–	–	**31.5 ± 3.4**
4	198652	90	3	Loam	10	25.1 ± 0.5	11.2 ± 0.3	65 ± 4	0.96 ± 0.05	1.90 ± 0.10	–	–	–	–	29.1 ± 2.5	23	–	–	**30.3 ± 3.2**
5	198653	110	4	Loess-like loam	10	29.8 ± 0.4	11.1 ± 0.2	32 ± 2	0.92 ± 0.04	1.86 ± 0.10	157.0 ± 10.8	7	209.1 ± 9.3	8	93.5 ± 6.8	20	80.2 ± 7.2	112.4 ± 8.0	**101.4 ± 9.3**
6	198654	150			10	31.5 ± 0.4	10.8 ± 0.4	41 ± 3	0.96 ± 0.05	1.90 ± 0.10	–	–	–	–	91.2 ± 7.7	16	–	–	**94.8 ± 9.8**
7	198655	200			10	29.0 ± 0.3	9.2 ± 0.2	28 ± 3	0.85 ± 0.04	1.79 ± 0.09	147.3 ± 15.1	8	210.7 ± 14.4	7	83.9 ± 7.5	13	81.9 ± 8.7	117.9 ± 10.8	**98.8 ± 10.8**
8	198656	220	5	Sandy loam	10	30.8 ± 0.8	10.5 ± 0.6	47 ± 8	0.98 ± 0.05	1.92 ± 0.10	111.5 ± 6.5	7	212.6 ± 12.8	8	97.4 ± 6.0	19	58.3 ± 4.2	110.8 ± 9.3	**99.3 ± 8.4**
9	198657	230		Sand	5	30.5 ± 0.5	24.5 ± 0.3	247 ± 5	0.87 ± 0.04	1.81 ± 0.09	124.5 ± 9.8	9	219.4 ± 11.0	10	80.8 ± 7.9	15	69.2 ± 5.6	121.4 ± 8.8	**92.9 ± 10.6**
10	198658	250			5	25.5 ± 0.6	7.0 ± 0.4	28 ± 6	0.82 ± 0.04	1.75 ± 0.09	–	–	178.1 ± 19.8	10	73.9 ± 8.2	14	–	101.6 ± 13.2	**90.7 ± 11.6**
11	198659	270			5	27.7 ± 0.5	7.3 ± 0.3	51 ± 4	0.91 ± 0.04	1.85 ± 0.09	–	–	–	–	87.1 ± 4.9	13	–	107.2 ± 17.4	**95.4 ± 7.1**
12	198660	290	6	Silt	20	35.9 ± 0.7	23.6 ± 0.5	260 ± 8	1.68 ± 0.08	2.61 ± 0.10	–	–	277.6 ± 36.7	11	–	–	–	**106.1 ± 16.7**	–
13	198661	320			20	38.2 ± 0.8	40.5 ± 0.7	503 ± 14	2.30 ± 0.11	3.24 ± 0.31	199.2 ± 4.3	8	326.3 ± 16.1	8	–	–	61.1 ± 4.3	**101.0 ± 8.6**	–
14	198662	340	7	Sand	5	49.4 ± 1.2	26.7 ± 0.8	275 ± 14	2.31 ± 0.13	3.24 ± 0.13	220.9 ± 4.3	7	352.8 ± 15.3	7	–	–	67.3 ± 3.0	**108.8 ± 6.7**	–
15	198663	360	8	Silt	20	28.7 ± 0.6	52.8 ± 0.6	697 ± 10	3.14 ± 0.14	4.07 ± 0.27	238.2 ± 5.4	8	503.5 ± 18.0	7	–	–	62.2 ± 4.6	**123.5 ± 9.4**	–
16	198664	390	9	Sand	5	48.0 ± 0.5	24.5 ± 0.4	247 ± 7	1.85 ± 0.14	2.67 ± 0.11	214.3 ± 5.4	8	372.5 ± 7.2	8	–	–	76.9 ± 5.5	**133.7 ± 9.4**	–
17	198665	410			5	30.0 ± 0.7	20.9 ± 0.8	231 ± 9	1.73 ± 0.09	2.54 ± 0.11	194.8 ± 7.6	8	361.1 ± 8.8	8	–	–	72.9 ± 3.9	**135.5 ± 6.5**	–

Table 2
Summary of luminescence data for the Eltigen section's outcrop B.

No	Sample code	Depth, cm	Unit	Lithology	WC, %	^{226}Ra, Bq kg^{-1}	^{232}Th, Bq kg^{-1}	^{40}K, Bq kg^{-1}	Dose rate, Bq ka^{-1} Quartz D_r, Bq ka^{-1}	Feldspar D_r, Bq ka^{-1}	IR$_{50}$ De, Gy	n	pIRIR$_{290}$ De, Gy	n	OSL De, Gy	n	IR$_{50}$ age, ka	n	pIRIR$_{290}$ age, ka	OSL age, ka
1	170831	280	4	Loess-like loam	10	29 ± 1.1	30 ± 0.9	355 ± 15	2.14 ± 0.11	3.07 ± 0.15	148 ± 3	12	223 ± 8	12	146 ± 8	12	48 ± 3	19	73 ± 4	69 ± 5
2	170832	480	6		10	33 ± 0.6	35 ± 0.7	406 ± 11	2.42 ± 0.12	3.36 ± 0.16	159 ± 11	8	268 ± 8	8	176 ± 17	8	47 ± 4	19	80 ± 4	73 ± 9
3	170833	520	7	Sand	5	17 ± 0.2	15 ± 0.2	98 ± 2	0.98 ± 0.04	1.92 ± 0.09	113 ± 24	5	236 ± 21	5	103 ± 4	5	59 ± 12	24	123 ± 12	105 ± 6
4	170834	630	8		5	15 ± 0.3	9 ± 0.3	103 ± 5	0.84 ± 0.03	1.78 ± 0.09	167 ± 10	6	238 ± 8	6	86 ± 4	6	94 ± 7	17	133 ± 8	103 ± 7
5	170835	880			5	15 ± 0.5	6 ± 0.5	72 ± 6	0.69 ± 0.03	1.63 ± 0.09	107 ± 5	6	216 ± 9	6	83 ± 4	6	66 ± 5	22	133 ± 9	121 ± 9
6	170836	920	9		5	12 ± 0.2	7 ± 0.1	84 ± 1	0.68 ± 0.03	1.61 ± 0.08	122 ± 11	6	216 ± 11	6	85 ± 2	6	76 ± 7	19	134 ± 9	127 ± 7
7	170837	1080			5	8 ± 0.4	7 ± 0.4	37 ± 8	0.46 ± 0.03	1.39 ± 0.08	97 ± 4	6	190 ± 9	6	58 ± 2	6	70 ± 5	22	136 ± 10	129 ± 10
8	170838	1180			5	28 ± 0.5	10 ± 0.4	42 ± 5	0.85 ± 0.04	1.79 ± 0.09	146 ± 9	12	245 ± 16	12	110 ± 5	12	82 ± 6	20	137 ± 11	130 ± 9

lagoonal silts (units 6, 8, 10). The age of the loess-soil sequence (units 1–4) lies in the range of 9 ± 1–99 ± 8 ka (Table 1, Fig. 5). The age of the marine sediments is in the range of 91 ± 12–136 ± 7 ka, and in the sequence of interlayered lagoonal and coastal-marine sediments, three groups of dates corresponding to three sedimentation cycles are distinguished: 1) in unit 9 (sand) with age of 136 ± 7 ka (Table 1, Fig. 5); 2) in units 8 (silt) and 7 (sand) in the range of 109 ± 8–134 ± 9 ka (Table 1, Fig. 5); 3) in units 6 (silt) and 5 (sand — sandy loam) with a range of 91 ± 12–106 ± 17 ka (Table 1, Fig. 5).

The inversion of dates likely results from the high sedimentation rate (Tables 1 and 2). However, the results remain valid within the confidence interval and stratigraphy.

4.2. Tuzla section

The Tuzla section (N45°11′57.87 E36°35′59.23) is an abrasion scarp (Fig. 7a), which rises to 12–14 m above sea level (Fig. 7b). The coast abruptly drops into the Kerch Strait and then gradually rises into a terrace-like surface that reaches up to 15–17 m in height near Cape Tuzla. This surface is gently undulating and contains faulted Miocene clays from the Sarmatian stage at its base (Pilipenko and Trubikhin, 2012). The section displays a thickness of marine sediments from the Karangatian transgression, overlaid by loess-like loams up to 7–8 m thick with three paleosols that are poorly developed (units 1–7). The loess soil sequence has a colour from dark brown (Holocene soil) to pale, characterised by columnar separation, sediment blocks, and carbonate nodules. Karangatian deposits in the section are represented by a thickness of 2.2 m (units 8–13).

In the Tuzla section, the following units are distinguished (Kurbanov et al., 2020): (9) dark grey silty sand (Fig. 7c, interval 8.00–8.25 m) with small shell detritus and whole shells of marine molluscs; (10) dark grey, heterogeneous, detrital sand (8.00–8.40 m) with rare marine mollusc shells; (11) reddish-grey, fine-medium-grained, horizontally layered sand (8.00–9.55 m) with interlayers of shells of marine molluscs, in the roof there is a ferruginous layer with thin-valve shells, in the middle of the unit a large fragment (up to 40 cm on the long side) of coquina was found; (12) grey, fine-grained to medium-grained sand (9.55–10.18 m), fine horizontal interlayering: alternating grey layers and red/-ferruginous layers with interlayers of detritus and layers of marine molluscs shells; the roof is highly ferruginous. Under this unit, separated by a sharp boundary, lies unit 13 of dark grey light loams with traces of ferruginization.

The results of the malacofaunal analysis of the Tuzla section (Kurbanov et al., 2020) have been revised and presented in Figs. 8 and 9. Supplementary Table 2 presents a complete list of species that comprise the outcrop's malacofaunal complexes and their ecological preferences.

At the lower part of the section at a depth of 9.95–10.18 m (unit 12), euryhaline and moderately euryhaline species of molluscs are found (*Mytilus galloprovincialis, Solen vagina, Ostrea edulis*). Above, an increase in biodiversity is observed simultaneously with a decrease in the percentage of *Mytilus galloprovincialis*, euryhaline *Cerastoderma glaucum*, and *Abra segmentum*, which are becoming widespread. In the interval of 9.38–9.45 m (unit 11), there is a large amount of detritus in the inclusion. At a depth of approximately 8.90 m (unit 11), *Flexopecten glaber* and *Donax venustus*, characteristics of the peak phase of the Karangatian transgression, appear. Further up the section, *Cerastoderma glaucum, Spusula subtruncata, Chlamelea gallina,* and other euryhaline and moderately euryhaline species occur in the complex again. From a depth of 8.40 m (units 10, 9), the species diversity of molluscs decreases to max. three euryhaline species adapted to survive in shallow and highly dynamic conditions.

Sediments exposed in the Tuzla section were dated in 2019, and the results were reported in Kurbanov et al. (2020). The Tuzla section's geochronology was determined using luminescence dating on feldspars (pIRIR$_{290}$) due to the saturation of quartz in the samples. Nine samples were collected from the section, seven of which were from Karangatian
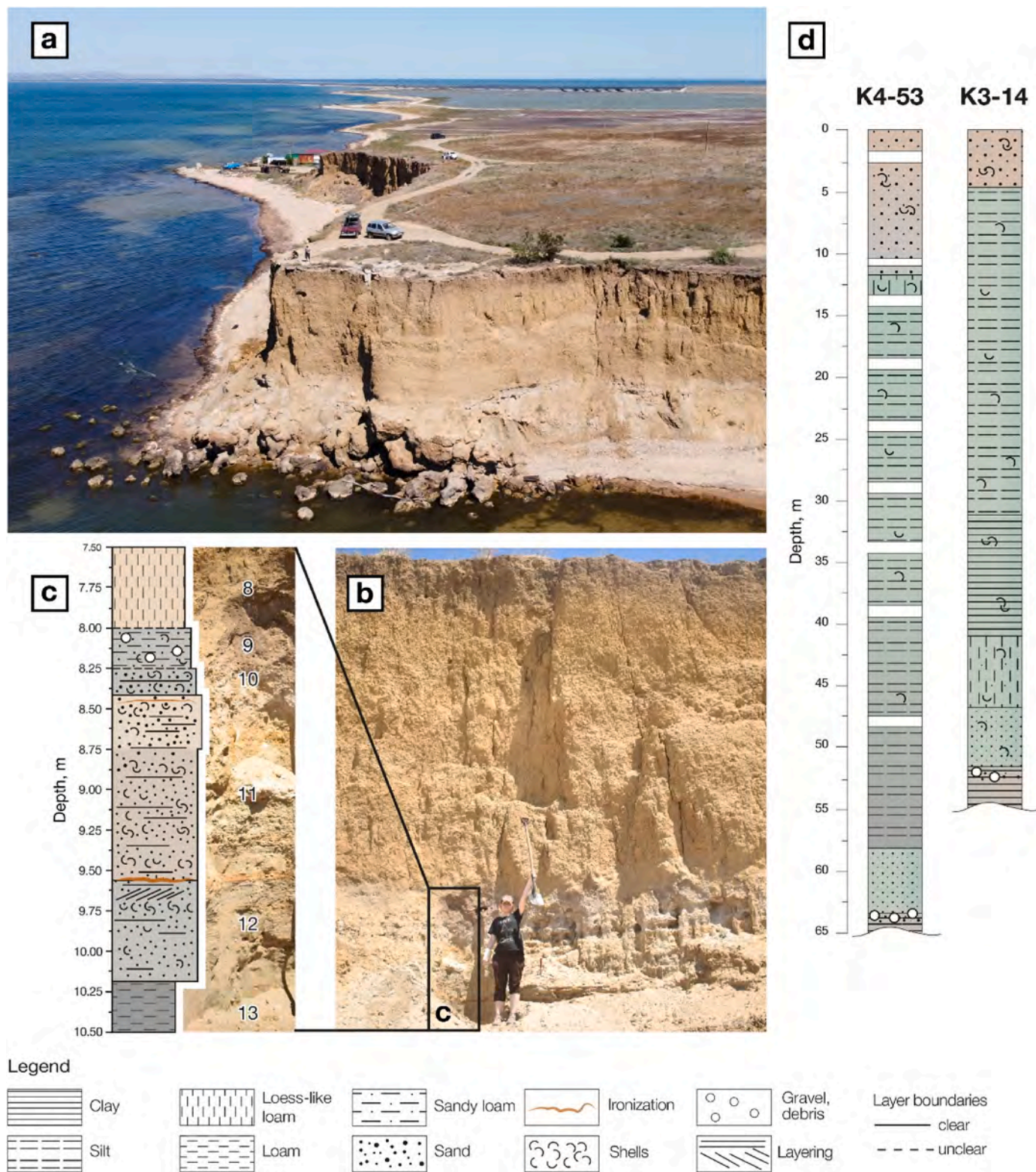
Fig. 7. (a) Tuzla section and (b, c) studied section outcrop, (d) boreholes lithological sections of Tuzla Island. Empty spaces on sections are gaps.

deposits (units 9–13) and two from the base of the overlying loess-soil sequence (unit 8). The results of luminescence dating of the Tuzla section are shown in Fig. 8 and are summarised in Table 3. Based on the luminescence dating results, two strata of different ages can be distinguished in the outcrop. The age of marine sediments ranges from 124 ± 8 to 127 ± 7 ka (Table 3, Fig. 8). The dates have a narrow range and, considering confidence intervals, almost identical values, indicating

high accumulation rates. The inversion date of 113 ± 7 ka (190894) is erroneous (Table 3, Fig. 8); the obtained age value is associated with overestimating the dose rate. A date of 108 ± 5 ka was obtained for sample 190888, collected from the poorly defined boundary between units 9 and 8 (Table 3, Fig. 8). The base of the horizon of loess-like loams (unit 8) is characterised by a date of 102 ± 6 ka (Table 3, Fig. 8).
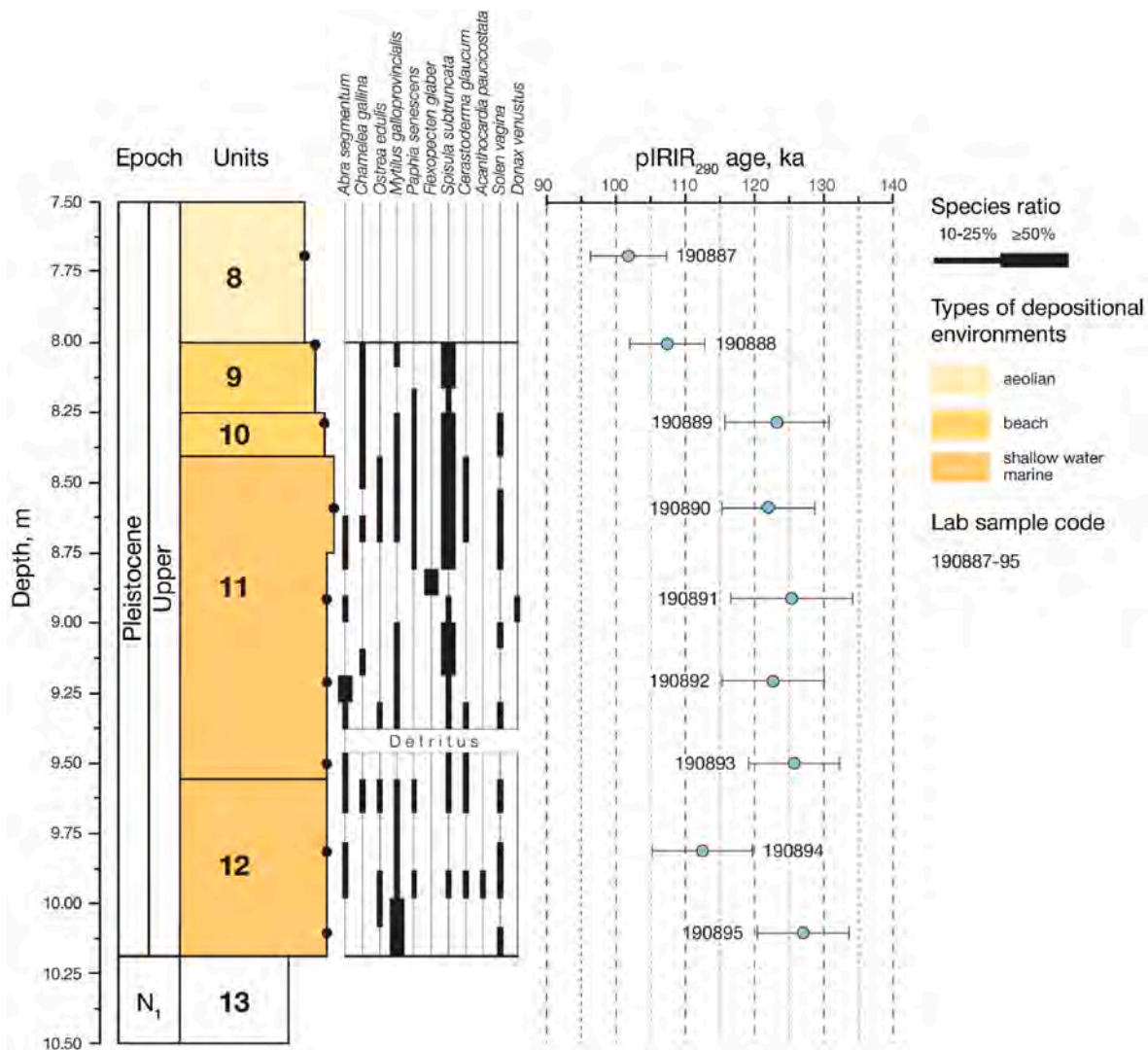
Fig. 8. Results of malacofaunal and geochronological analyses of the Tuzla section.

4.3. Boreholes of Tuzla Island

The study conducted a paleogeographic analysis of four boreholes, 93, 95, K4-53 and K3-14, drilled in different locations across Tuzla Island with depths ranging from 70 to 80 m (Semikolennykh et al., 2018). In borehole K3-14 the following deposits are revealed (Semikolennykh et al., 2018): (1) brown sandy-gravel biogenic unit (Fig. 7d, interval 0.0–4.0 m) with mollusc shells; (2) grey clayey silt (4.0–12.0 m), saturated with large molluscs shells; (3) greenish clayey silt (12.0–17.0 m) with small-valve mollusc shells (higher in the core the size of the shells increases); (4) green-grey clayey silt (17.0–20.0 m) with large mollusc shells; (5) grey-green clayey silt (20.0–29.0 m) with relatively large mollusc shells; (6) green-grey clayey silt (29.0–31.0 m) with lenses and veinlets of grey and dark grey silt with shell detritus; (7) grey-green dense silty clay (31.0–42.5 m) with lenses and layers of grey and dark grey silt with very small oppressed mollusc shells, higher up the core the size of the shells increases; (8) grey-green sandy silt (42.5–47.0 m) with silty lenses including shells of estuarine and freshwater molluscs; (9) greenish-light-grey fine-grained sand (47.0–51.5 m) with gravel and fragments of estuarine and freshwater molluscs shells; (10) dark brown dense clay exposed 18.5 m thick at the top with sand, gravel and shell detritus.

In borehole K4-53, the following deposits are revealed (Semikolennykh et al., 2018): (1) reddish-brown coarse-grained biogenic sand (Fig. 7d, interval 0.0–1.5 m); (2) brownish-beige heterogeneous sand (2.5–3.5 m) with gravel-pebble material and broken, small shells of molluscs; (3) dark grey to black medium-coarse-grained sand (3.5–5.5 m) saturated with shell detritus and small mollusc shells; (4) 5.5–10.5 m grey medium-fine-grained sand with shell detritus; (5) greenish-grey homogeneous silty sand (11.0–12.0 m); (6) greenish-grey homogeneous slightly clayey silt (12.0–13.0 m) with small mollusc shells; (7) greenish-grey clayey silt (14.0–18.0 m) with thin veins of light grey silt and with fairly large mollusc shells; (8) greenish-grey clayey silt (19.0–23.0 m) with mollusc shell; (9) greenish-grey clayey silt (24.0–28.0 m) with small fragments of mollusc shell; (10) greenish-dark grey clayey silt (29.0–33.0 m), unclearly layered with small mollusc shells; (11) dark grey to black clayey silt (34.0–38.0 m) with thin layers of grey silt with small closed valves of mollusc shells; (12) black dense clayey silt (39.0–43.0 m) with shell detritus; (13) green to dark grey to black clayey silt (43.0–48.0 m) with very small, oppressed fragments of mollusc shells; (14) grey-green clayey dense silt (49.3–53.0 m) with fragments of mollusc shells; (15) greenish-grey clayey unclearly layered silt (53.0–58.0 m) with plant remains, smoothly turning into light grey silt with interlayers of greenish-grey clayey silt; (16) greenish-light-grey fine-grained sand (58.0–63.5 m) saturated with shell detritus; (17) dark brown clay with sand, gravel in the roof and exposed thickness of 20.5 m.

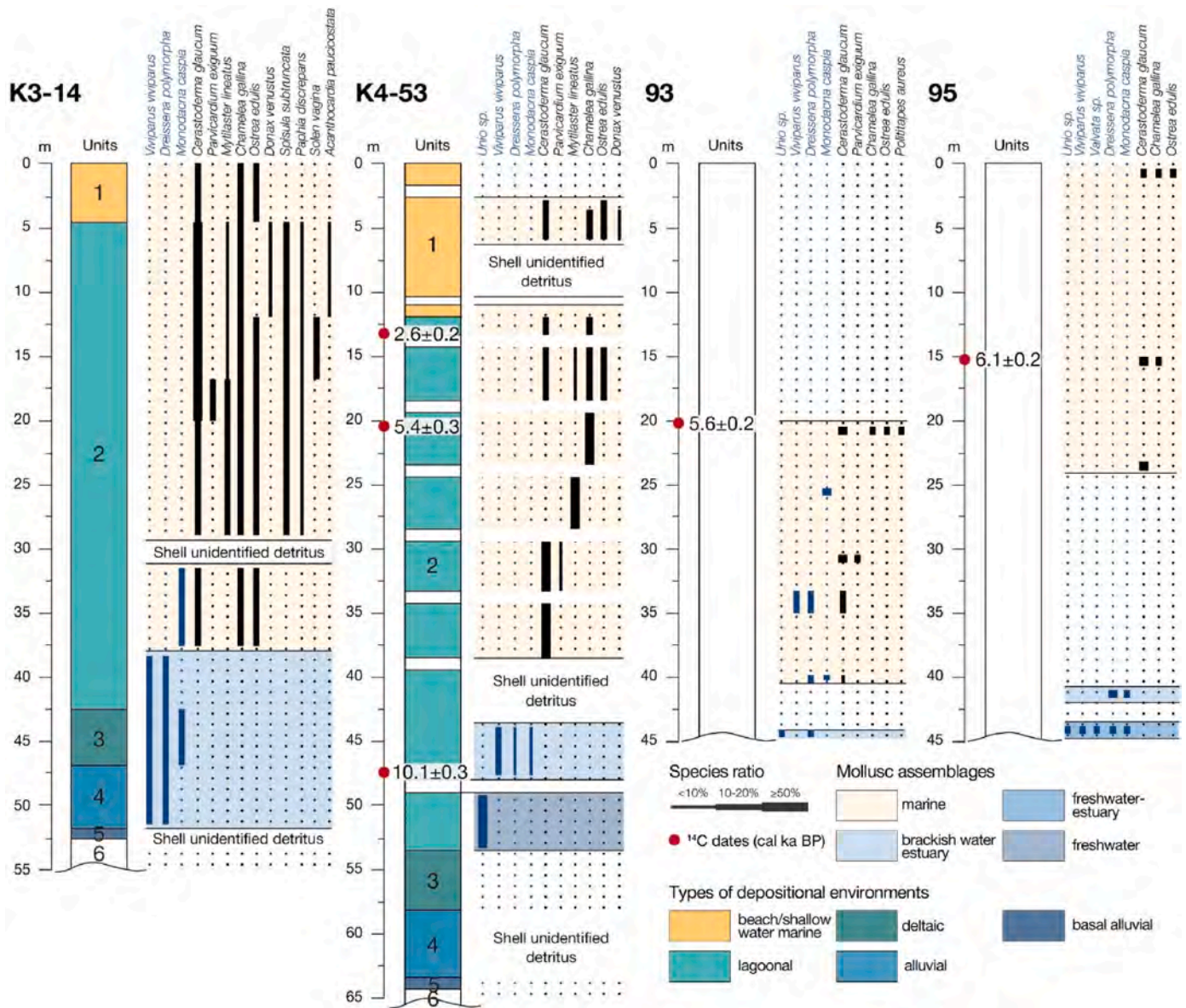The author did not have a lithological description of boreholes 93

Fig. 9. Results of malacofaunal and geochronological analyses of Tuzla Island boreholes. The White stripes on the K4-53 scheme indicate gaps in the core.

and 95. However, based on the structure description of boreholes K4-53 and K3-14 and literary data (Shnyukov et al., 1981), it can be assumed that all four cores have similar facies and lithological compositions.

The results of the malacofaunal analysis of borehole cores on Tuzla Island (Semikolennykh et al., 2018) are presented in Figs. 9 and 10. A complete list of species that make up the malacofaunal complexes of borehole cores and their environmental preferences are presented in Supplementary Table 3.

Malacofaunal analysis of the K3-14 borehole core showed that the malacofaunal complex at a depth of 47.0–51.5 m (unit 4) contains fragments of freshwater mollusc (*Viviparus viviparus*) shells and the brackish-water estuary species *Dreissena polymorpha*. In the interval of 42.5–47.0 m (unit 3), shells of brackish-water Caspian mollusc *Monodacna caspia* appear in the complex. Further up the core (unit 2), the freshwater-estuary complex is replaced by an estuary-marine complex: from a depth of about 37.0 m, small, oppressed shells of marine molluscs *Ostrea edulis*, *Cerastoderma glaucum*, *Chamelea gallina* appear, freshwater species disappear entirely. In the interval of 29.0–31.0 m (unit 2), shell fragments are present, but their identification with a specific species is impossible. Up to a depth of 4.0 m (unit 2), the species diversity of

molluscs increases, along with *Ostrea edulis*, *Chamelea gallina* and the predominant *Cerastoderma glaucum*, *Mytilaster lineatus*, *Paphia discrepans*, *Spisula subtruncata*, *Donax venustus* and other marine species appear, the size of shells increases. The species are depleted within the marine assemblage from a core depth of 4.0 m and higher (unit 1).

In borehole K4-53, fragments of freshwater mollusc species *Unio* sp. were found in the lowest strata at a depth of 49.3–53.0 m (unit 2). In the interval of 43.0–48.0 m (unit 2), small, depressed shells of brackish-water estuary species *Dreissena polymorpha* and *Monodacna caspia* are added to the freshwater *Viviparus viviparus*. The core interval of 39.0–43.0 m (unit 2) is characterised by shell detritus. From a depth of 38.0 m (unit 2), small shells of the marine mollusc *Cerastoderma glaucum* appear *in situ* in the sediments. Higher up the core, small shells of *Parvicardium exiguum* are added to the shells of *Cerastoderma glaucum*. In the core interval of 24.0–28.0 m (unit 2), only small fragments of *Mytilaster lineatus* shells were found. To a depth of 24.0 m (unit 2) and higher, more halophytic marine species of molluscs began to appear, such as *Chamelea gallina* and *Ostrea edulis*, and the size of the shells began to enlarge. From a core depth of about 12.0 m (unit 1), the species composition becomes depleted, and only the most tolerant to temperature fluctuations and the

Table 3
Summary of luminescence data for the Tuzla section.

No	Sample code	Depth, cm	Unit	Lithology	WC, %	^{226}Ra, Bq kg^{-1}	^{232}Th, Bq kg^{-1}	^{40}K, Bq kg^{-1}	Quartz D$_r$, Bq ka^{-1}	Feldspar D$_r$, Bq ka^{-1}	IR$_{50}$ De, Gy	n	pIRIR$_{290}$ De, Gy	n	OSL De, Gy	n	IR$_{50}$ age, ka	pIRIR$_{290}$ age, ka	OSL age, ka
1	190887	770	8	Loess-like loam	10	42.8 ± 1.0	44.5 ± 0.8	478 ± 16	3.1 ± 0.1	4.0 ± 0.2	261.3 ± 25.6	8	410.6 ± 13.2	8	–	–	64.8 ± 6.4	**101.9 ± 5.5**	–
2	190888	800	9	Sandy loam	10	17.4 ± 0.9	19.1 ± 0.8	500 ± 19	2.3 ± 0.1	3.2 ± 0.1	206.8 ± 7.3	8	344.8 ± 8.1	8	–	–	64.5 ± 3.5	**107.5 ± 5.4**	–
3	190889	830	10	Sand	5	13.5 ± 0.4	15.4 ± 0.4	435 ± 11	1.8 ± 0.1	2.8 ± 0.1	230.8 ± 22.9	8	342.3 ± 11.5	8	–	–	83.3 ± 8.6	**123.5 ± 7.5**	–
4	190890	860	11		5	11.8 ± 0.5	13.2 ± 0.4	422 ± 12	1.7 ± 0.1	2.7 ± 0.1	175.7 ± 3.2	8	324.6 ± 7.7	8	190.0 ± 7.5	33	65.8 ± 3.4	**121.6 ± 6.7**	109.7 ± 6.8
5	190891	890			5	14.6 ± 0.9	19.7 ± 0.8	451 ± 20	2.0 ± 0.1	2.9 ± 0.2	229.9 ± 26.7	8	362.7 ± 22.5	8	–	–	79.2 ± 9.4	**125.1 ± 10.5**	–
6	190892	920			5	15.1 ± 0.2	19.5 ± 0.2	453 ± 4	2.0 ± 0.1	2.9 ± 0.1	214.9 ± 12.3	7	356.9 ± 12.4	7	–	–	73.9 ± 5.2	**122.7 ± 7.4**	–
7	190893	950	12		5	11.8 ± 0.2	15.4 ± 0.2	494 ± 4	2.0 ± 0.1	2.9 ± 0.1	230.1 ± 22.1	9	364.5 ± 7.9	9	–	–	79.1 ± 8.0	**125.3 ± 6.6**	–
8	190894	980			5	18.4 ± 0.4	22.7 ± 0.4	654 ± 12	2.7 ± 0.1	3.6 ± 0.2	232.6 ± 24.2	9	404.7 ± 16.2	9	–	–	64.7 ± 6.9	**112.5 ± 7.2**	–
9	190895	1010	13	Loam	10	16.8 ± 0.9	20.3 ± 0.7	561 ± 19	2.3 ± 0.1	3.3 ± 0.2	206.8 ± 2.7	9	412.9 ± 7.3	9	–	–	63.4 ± 3.2	**126.7 ± 6.6**	–

Table 4
Radiocarbon dating results (after Semikolennykh et al., 2018).

Sample ID	Borehole	Depth, m	Material	^{14}C age, yr BP	Calibrated age, yr BP
LU-8428	K4-53	2.5–13.0	Shell *Cerastoderma glaucum*	2510 ± 120	2590 ± 150
LU-8429	K4-53	20.1–20.3	Shells *Chlamelea gallina, Viviparus viviparus*	4720 ± 200	5360 ± 300
LU-8430	K4-53	47.5–47.8	Shells *Viviparus viviparus*	8990 ± 240	10060 ± 340
LU-8108	93	20.0–20.1	Shells *Cerastoderma glaucum, Chlamelea gallina*	4810 ± 100	5590 ± 160
LU-8110	95	15.0–15.1	Shells *Cerastoderma glaucum, Chlamelea gallina*	5240 ± 120	6050 ± 140

dynamics of the reservoir species *Cerastoderma glaucum* and *Chamelea gallina* remain. In the core interval of 3.5–5.5 m (unit 1), the assemblage includes *Cerastoderma glaucum*, *Chamelea gallina* and small valves of *Ostrea edulis* shells and *Donax venustus*.

In boreholes 93 and 95 cores, the mollusc fauna is represented fragmentarily. In borehole 93 at a depth of 44.0–44.2 m, there are freshwater *Unio* sp. and brackish-water species *Dreissena polymorpha*. In the interval of 40.0–40.3 m, small shells of the marine mollusc *Cerastoderma glaucum* appear along with Caspian brackish-water *Monodacna caspia*. At 33.0–35.0 m depth, estuary *Dreissena polymorpha*, marine *Cerastoderma glaucum* and freshwater species *Viviparus viviparus* are present. However, in the core interval of 30.0–30.1 m, only marine species *Cerastoderma glaucum* (predominant) and *Parvicardium exiguum* are found. At 25.0–25.2 m depth, only fragments of *Monodacna caspia* are found in the sediments. In the core interval 20.0–20.2 m, shells of two marine molluscs, *Ostrea edulis* and *Polititapes aureus,* were discovered.

In borehole 95 at a depth of 43.5–43.6 m, fragments of freshwater species *Viviparus viviparus*, *Unio* sp., *Valvata* sp. and valves of brackish-water species *Monodacna caspia* and *Dreissena polymorpha* were found. In the interval of 41.0–41.1 m, only estuary brackish-water species *Monodacna caspia*, and *Dreissena polymorpha* (predominant) were found. At a depth of 23.0–23.1 m, small, depressed shells of the marine species *Cerastoderma glaucum* appear *in situ*. At a depth of 0.8–1.0 m, shells of *Ostrea edulis* were added to the marine assemblage.

The results of radiocarbon dating are shown in Fig. 9 and presented in Table 4. According to the results of radiocarbon dating of borehole cores, the lower horizons, including the Neoeuxinian malacofaunal complex, accumulated at the Late Pleistocene — Holocene boundary. The change of freshwater sedimentation regime to estuary occurred approximately 11–10 cal ka BP. The appearance and spread of marine species of molluscs correlate with the Holocene Epoch.

5. Discussion

5.1. Sedimentary environments of the study sections

5.1.1. Eltigen section

The analysis results revealed three sedimentation phases during the Karangatian transgression, evident in the Eltigen section (Fig. 5). The first phase corresponds to shallow lagoon sediments accumulation with the poor species composition of euryhaline molluscs in the eastern part of modern Lake Tobechik. The second phase corresponds to the accumulation of lagoonal and coastal-marine sediments with euryhaline molluscs in the southern part and the thick strata of coastal-marine sediments with the most thermophilic and halophytic Mediterranean

Fig. 10. Species found in boreholes of Tuzla Island.

species of molluscs in the central part of the section. During the third phase of the transgression, lagoonal — shallow marine and low-thickness beach sediments accumulated with euryhaline and moderate euryhaline molluscs in the southern and central parts of the section, respectively. According to OSL dating, the sedimentation time of the three phases of the Karangatian transgression is in the range of ~130–95 ka BP (Tables 1 and 2, Fig. 5). The subaerial strata accumulation started at around 100–90 ka BP (Table 1, Fig. 5). The age of the lower paleosol in the central part of the section is estimated to be ~80–70 ka BP (Table 2, Fig. 5). The second paleosol accumulation began no earlier than 69 ± 5 ka BP (Table 2, Fig. 5). A thin unit of colluvium in the southern part of the section has an age of 30 ± 3 ka (Table 1, Fig. 5).

Several researchers (Nevesskaya, 1965; Zubakov, 1988; Yanko et al., 1990; Dodonov et al., 2000; Chepalyga, 2002; Shelkoplyas and Khristoforova, 2007; Svitoch, 2009) attributed the deposits of the southern part of the Eltigen section, characterised by alternating sandy units with silt, to the first phase of the Karangatian transgression. However, it was determined that only the lower strata of the outcrop could be attributed to the early phase based on the results of OSL dating (Table 1, Fig. 5). Facies differences within the section reflect different depositional environments. This fact indicates the nonlinearity of the development of the Karangatian transgression against the background of the difference in the rates of tectonic uplift with increasing distance from the axis of the anticlinal fold, in the flank of which the section is located and the action of local relief-forming factors. Only two datings are known, obtained from sediments in the southern part of the section: U/Th date of 127 ± 9 (Dodonov et al., 2000) and TL date of 205.0 ± 50.0 (Zubakov, 1988). The first dating does not contradict the results of OSL dating, given that there is no exact description of the sampling site; the second sedimentation cycle, identified in the southern part of the section, is indeed of a similar age. The second date with a confidence interval of 50 ka years can hardly be considered informative. In general, the dating results of the marine sediments section using the U/Th method (Arslanov et al., 1972, 1983) showed a range of dates between 127 and 58 ka BP. Notably, most dates fall within the 127–90 ka range, generally

consistent with OSL dating results (Tables 1 and 2). However, it is impossible to identify separate U/Th age intervals in the strata due to the absence of any pattern in the distribution of dates.

The upper unit of the oblique and horizontally layered sands in the section's central part presents a unique challenge (Fig. 5). It cannot be classified as belonging to the Tarkhankutian stage (Nevesskaya, 1965; Yanko et al., 1990) of basin development, nor can it be compared with those from the Surozh transgression (Zubakov, 1988). According to the results of OSL dating, the upper unit of the central part of the section corresponds to the 110–100 ka BP age interval (Table 2, Figs. 2 and 5). This finding adds a new layer of complexity to our understanding of the area's geological history. It correlates with the third, upper Karangatian phase (Svitoch, 2009).

Previously, the continental sediments of the Eltigen section had not been dated. Only one date, 50.2 ka, was obtained using the TL method at the boundary of marine and continental sediments (Zubakov, 1988).

5.1.2. Tuzla section

The Tuzla section represents a sequence of coastal-marine sediments accumulated in a relatively warm and shallow basin (Fig. 8). The stratum with erosion lies on silent loams, possibly of the same age of lagoonal origin. Fedorov (1963) found oppressed shells of *Cerastoderma glaucum* in the composition of these loams, the presence of which, in his opinion, indicates the existence of a desalinated lagoon in the area of the Tuzla section, influenced by river waters, at the beginning of the Karangatian Epoch. Chronologically, marine deposits of the Tuzla section correspond to the second phase of the Karangatian transgression (MIS 5e), identified in the Eltigen section (Table 3, Fig. 8). This conclusion is partially consistent with the findings of Svitoch (2009), who inferred that the Karangatian deposits of the section accumulated in a shallow and warm basin and can be correlated with only one of the phases of the Karangatian transgression.

The upper stratum, dated 108 ± 5 ka BP (Table 3, Fig. 8), contains marine species. However, it is heavily reworked by aeolian and pedogenesis processes, reflected in many silty filler and carbonate nodules.

The only previously obtained OSL date of 85 ± 6 ka for the upper part of marine sediments (Pilipenko and Trubikhin, 2012) is outside the allocated range of marine sediments accumulation, which may be because the sample was collected from a different outcrop, and the degree of erosion of the upper boundary of the deposits may vary along the section.

Subaerial sedimentation started here at around 100 ka BP (Table 3, Fig. 8). According to the results of previously conducted paleomagnetic studies, the upper two soils correspond to the Bryansk interstadial (MIS 3), and the age of the second soil, along with the underlying loess, at a depth of 2.6–4.2 m, is estimated to be 35–25 ka (Pilipenko and Trubikhin, 2012).

5.1.3. Boreholes of Tuzla Island

Quaternary sediments observed in the boreholes overlie the dark brown Neogene clays with a sharp erosional boundary (Semikolennykh et al., 2018) (Fig. 9). The lower strata in the interval of 47.0–51.5 m of the borehole K3-14 core and the interval of 58.0–63.5 m of the borehole K4-53 core is of alluvial origin. Its base is represented by a mixture of sand and gravel with shell detritus. The main part of the strata is composed of fine-grained sand. Further up, the cores revealed a unit of clay and silt unit which is more than 40 m thick and enriched in organic matter, especially in its lower half and containing mollusc shells. These deposits correspond to the estuary, deltaic and lagoonal sedimentary environments with signs of short-term activation of fluvial processes, indicated by the presence of coarser material layers in the silts and detritus of mollusc shells. The upper unit of sand and sand-gravel deposits in borehole cores indicates a dynamic coastal-marine sedimentary environment similar to the modern one.

Two significant malacofaunal complexes were identified in the boreholes' sections (Fig. 9). The first is the Neoeuxine complex, comprising fresh and brackish water estuary species, and the second is the Chernomorian (Black Sea) with euryhaline marine species. The Neoeuxinian complex in the Kerch Strait can be divided by species composition into freshwater, freshwater-estuary and brackish water-estuary sub-complexes, the change of which occurs linearly in the sediments. One of the Neoeuxinian complex features is the presence of brackish-water molluscs *Monodacna caspia* in its sub-complexes.

Radiocarbon analysis of mollusc shells has allowed us to determine that the Neoeuxinian strata accumulated during the transition from the Late Pleistocene to the Holocene (Table 4, Fig. 9). Additionally, the appearance of Caspian species in the malacofaunal complex within the Kerch Strait can be traced back to 11–10 ka BP (Table 4, Fig. 9). Chernomorian (Black Sea) sediments accumulated during the Holocene Epoch. The transition to a coastal-marine sedimentation environment close to the modern one occurred at about 2.6 ka BP (Table 4, Fig. 9).

5.2. Late Pleistocene-holocene palaeogeographic evolution of the Kerch Strait

5.2.1. Karangatian transgression (MIS 5e–c)

The Black Sea experienced the Karangatian transgression after the Uzunlarian regression (Yanina, 2012). Three phases of the transgression, separated by brief regressions, were identified in the Kerch Strait (Fig. 11b–d).

The first phase (MIS 6-5e)

During the initial stage of transgression (Fig. 11b), the estuary malacofaunal complexes inherited from the Uzunlarian Basin and living in the waters of the Kerch Strait and adjacent reservoirs were replaced by marine complexes. These complexes characterise the water salinity of
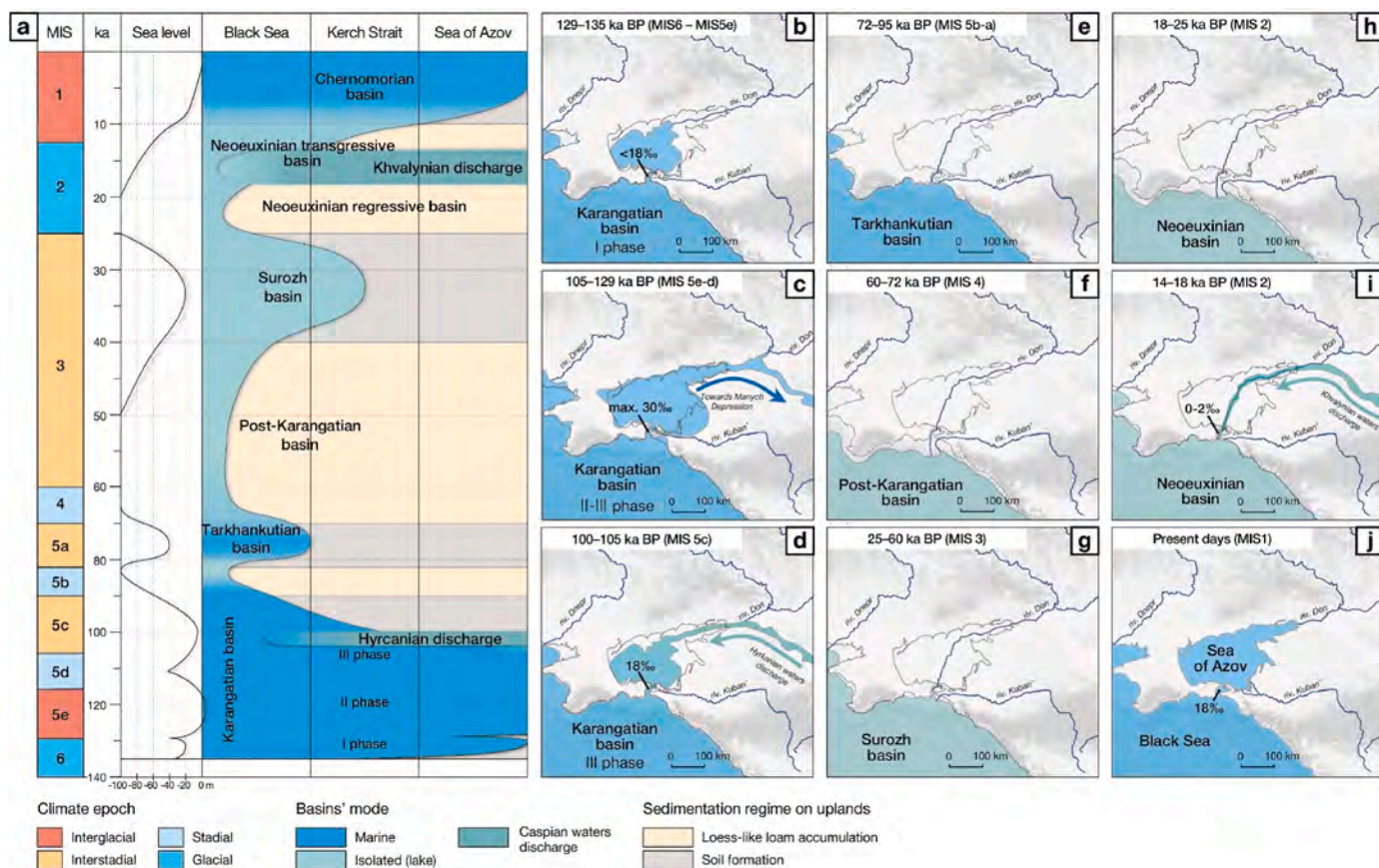

Fig. 11. The scheme of the general water level and environmental changes in the Black Sea, Kerch Strait and Sea of Azov (a) and palaeogeographic reconstruction (b–j) of the main stages of the Kerch Strait development with adjacent basins in the late Quaternary. The Pont water level is drawn using data from Balabanov and Izmailov (1988), Chepalyga (2002), Sorokin (2011), and Yanina (2012).

<12‰.

The spore-pollen spectra found in the Lower Karangatian deposits in a borehole in the vicinity of Cape Kazantip (Sea of Azov) suggest that during that period in the Kerch Peninsula, forb steppes were widespread on elevated terrains and mixed forests consisting of oak and pine trees could be found along river valleys and ravines (Semenenko and Sidenko, 1979). This indicates that the climate was relatively warm during this period. Detailed pollen records from the SE Black Sea shelf also reconstructed the initial warming in Northern Anatolia on the edge of MIS 6 and MIS 5e, at ~130.4 ka (Shumilovskikh et al., 2013b).

OSL dating, considering confidence intervals, obtained for the Lower Karangatian deposits of the Eltigen section determined the age of sedimentation at ~130 ka BP (Tables 1 and 2, Fig. 5). This time interval marks the transition from the Moscow (Saalian) glaciation (MIS 6) to the Mikulino (Eemian) interglacial (MIS 5e) on the East European Plain. Marine malacofauna assemblages indicate the Mediterranean waters' penetration into the Kerch Strait due to the interglacial transgression of the World Ocean onset (Lisiecki and Stern, 2016). The MIS 6-5e transition to marine conditions in the Sea of Marmara was dated at ~134.06 ± 1.10 ka BP (Çağatay et al., 2019). A multi-proxy study of the borehole sediments on the Black Sea's SE shelf, dated to ~128 ka BP (Shumilovskikh et al., 2013a; Wegwerth et al., 2014), established the beginning of Mediterranean waters' penetration into the Black Sea, consistent with this study's data.

The decrease in the water level of the Karangatian Basin in the Kerch Strait is marked by an erosional unconformity in sedimentation in the Eltigen section's central part and a change from a shallow-coastal-marine environment to a lagoonal/estuary environment in its southern part (Fig. 5). This event may reflect a short-term global cooling during 131–129 ka BP (Wegwerth et al., 2019) similar in dynamics to the Younger Dryas.

The second phase (MIS 5e-d)

During the second phase of transgression, the salinity of the Kerch Strait and the adjacent water area was in the range of 12–18‰ (Fig. 11c). The strait at that time was wider and deeper than the modern one (Chepalyga, 2002). All large estuaries were flooded, and Tuzla and Chushka spits did not exist in the strait's water area (Shnyukov et al., 1981). The transgression penetrated far to the east into the Manych Depression (Semikolennykh et al., 2023b).

Some water desalination was observed in the Kerch Strait near Lake Tobechik and Cape Tuzla due to the composition of the malacofauna species. The salinity of the water did not exceed 20‰. The results of seismic profiling of Taman Bay made it possible to characterise the Karangatian age strata 15 m below sea level as alluvial sediments (Gaydalenok et al., 2019). Probably, the eastern part of the Kerch Strait could have been desalinated through the influence of the waters of the paleo-Kuban River, which flows into the Taman Bay, as Fedorov (1963), Nevesskaya (1965) and Svitoch (2009) wrote about. According to mineralogical analysis, it was established that the formation of sandy deposits of the Karangatian transgression in the Tuzla section was determined by the supply of clastic material with the runoff of the Kuban River (SHii and Rostovtseva, 2013). Desalination in the Lake Tobechik area could result from the flow of numerous gully watercourses into its basin.

According to the results of OSL dating, the second-phase sediments accumulated in the interval 129–115 ka BP (Tables 1–3, Figs. 5 and 8). This period corresponds with the warm Mikulino (Eemian) interglacial period (MIS 5e). The Azov region used to be covered with typical steppe vegetation similar to the modern (Velichko et al., 2012). The steppe zone was also reconstructed in the south of the East European Plain (Markova, 2000; Kaytamba, 2005). Pollen records from the SE Black Sea shelf reconstructed higher than present summer temperatures (significant spread of *Fagus*) between 126.4 and 122.9 ka in Northern Anatolia (Shumilovskikh et al., 2013b) and warm and fully marine sea-surface conditions in the Black Sea between 126.5 and 121.0 ka with sea-surface salinity >28‰ (Shumilovskikh et al., 2013a).

The estimated sea level of the Mediterranean Basin during MIS 5e, according to various data (Wegwerth et al., 2014; Sivan et al., 2016; Gzam et al., 2016; Polyak et al., 2018; Salonen et al., 2018; Marra et al., 2020) is 1–9 m above the present sea level. Globally, during the MIS 5e, the climate was warm, and the World Ocean level could have been 9 m higher than the current level (Dutton et al., 2015; Tzedakis et al., 2018). The Karangatian deposits with a Mediterranean faunal complex, reflecting the peak of the transgression, are not found below modern sea level (Shnyukov et al., 1981). However, all discovered coastal outcrops of Karangatian sediments are located within uplifted terraces; hence, the level of the Karangatian Basin in MIS 5e could reach elevations in the range of 1–9 m, similar to the Mediterranean Sea.

The third phase (MIS 5c)

After a relatively short-term regressive retreat of the coastline during the Kurgolovo cooling (MIS 5d) of the Valdai glaciation, the Kerch Strait was occupied by the waters of the third — final phase of the Karangatian transgression (MIS 5c) (Fig. 11d). The salinity of the strait water reached 28–30‰.

Based on the hypsometric position, thickness, and structure of the Karangatian deposits exposed in the coastal outcrops of the Kerch Strait (Figs. 5 and 8), the influence of tectonic uplift of varying intensity can be traced. For example, deposits of the third transgression phase are not found in the Tuzla section, which may be due to high rates of tectonic uplift (Rogozhin et al., 2015) — the waters of the third phase did not reach the previously formed marine terrace. After the coastline retreat at the end of the Mikulino (Eemian) interglacial (MIS 5e), the area of Cape Tuzla entered the continental development phase (Table 3, Fig. 8).

The Kerch Strait was occupied by the waters of the third phase of the Karangatian transgression ~110–95 ka BP, as indicated by OSL dating of sediments from the Eltigen section (Tables 1 and 2). The beginning of the third phase of the Karangatian transgression coincided (Kurbanov et al., 2018) with the Hyrcanian waters (Yanina, 2014) flowing through the Manych Depression and the Kerch Strait into the Black Sea from the Caspian Sea (Yanina et al., 2024). The Hyrcanian runoff continued until 100 ka BP (Kurbanov et al., 2018). The introduction of brackish water from the Caspian Sea significantly reduced the salinity of the Kerch Strait, which is reflected in the composition of the fauna.

The third Karangatian stage corresponds to MIS 5c (Upper Volga interstadial on the East European Plain) (Tables 1 and 2). Global warming led to rising sea levels (Lisiecki and Stern, 2016). The level of the Mediterranean Sea did not exceed 0–3 m above the present sea level (Marra et al., 2020) or was even lower. In the Azov region (Velichko et al., 2017), horizons of paleosols that correspond to the distribution of dry steppes in this territory were identified. The final retreat of the Karangatian Basin's waters around the Eltigen section dates back to ~95–90 ka BP, which refers to the beginning of the Lapland cooling on the East European Plain (MIS 5b) (Tables 1 and 2, Fig. 5). Loess-like loams began accumulating on the strait coast. During the Lapland stadial (MIS 5b), the Black Sea level may have been as low as −35 to −40 m or even lower since the Sea of Marmara bottom sediments, which correspond to the communication cessation stage with the regressing Mediterranean Sea, were recorded at the same depths (Çağatay et al., 2019) (Fig. 11e). The Kerch Strait's marine sedimentation regime transitioned to an estuary and later to an alluvial environment (Shnyukov et al., 1981).

5.2.2. Tarkhankutian transgression (MIS 5a)

The connection between the Black Sea, Sea of Marmara and Mediterranean Sea by the beginning of the Kruglitsa interstadial (MIS 5a) resumed (Badertscher et al., 2011; Çağatay et al., 2019). Most likely, a relatively minor transgression of the World Ocean and, accordingly, the Mediterranean Sea during the Kruglitsa interstadial (MIS 5a) led to the formation of the Tarkhankutian Basin (Fedorov, 1963; Nevesskaya, 1965; Yanina, 2012) in the Black Sea. The level of the Black Sea at this time rose to −35 to −20 m (Nevesskaya and Nevessky, 1961; Sorokin, 2011; Svitoch and Makshaev, 2017), and its salinity, based on

malacofaunal complexes with depleted euryhaline Mediterranean species, was below 14–15‰ (Yanina, 2012). Marine sediments of this stage were not found in the Kerch Strait and the adjacent waters; most likely, they were eroded during subsequent regressive phases (Fig. 11e). During this period, the soil overlying loess-like loams accumulated on the strait coast in MIS 5b (Table 2, Fig. 5).

5.2.3. Post-Karangatian regression (MIS 4)

During the onset of global cooling during MIS 4, the Black Sea's water level dropped significantly down to a range from −70 to −100 m (Sorokin, 2011; Yanina, 2012). This caused the Black Sea to become isolated from the Mediterranean Sea (Hoyle et al., 2021), which also experienced a decrease in its water level (Ballesteros et al., 2017; Benjamin et al., 2017) along with the overall level of the World Ocean (Spratt and Lisiecki, 2016). The sharp decline in sea level was accompanied by intense erosion. There was a deep incision to the Neogene base in most of the Kerch Strait area (Shnyukov et al., 1981) (Fig. 11f). Large ravines such as Tobechikskaya formed during this period (Blagovolin, 1960). The accumulation of loess-like loams continued on the coast of the strait (Tables 1 and 2, Fig. 5).

5.2.4. Surozh transgression (MIS 3)

Due to the extensive erosion of the Kerch Strait's bottom during the Late Valdai regression, it is impossible to identify deposits of the Bryansk interstadial (MIS 3) and the associated Surozh transgression of the Black Sea (Popov, 1983; Yanina and Sorokin, 2022). A suggestion that the Surozh Basin of the Black Sea had no connection with the Mediterranean Sea was proven by drilling data on the Black Sea (Shumilovskikh et al., 2014) and the Sea of Marmara (Çağatay et al., 2009; Büyükmeriç et al., 2016) shelves. The sea level could rise due to increased precipitation and riverine inflow against the backdrop of global warming and/or sea level rise could be associated with the discharge of the Caspian Sea waters (Shumilovskikh et al., 2014; Yanina and Sorokin, 2022). Popov (1983) identified sediments of the Surozh Basin on the bottom of the Kerch Strait based on mollusc fauna. He listed Khvalynian (*Didacna ebersini, D. subcatillis, Monodacna caspia, Dreissena polymorpha*), Mediterranean (*Cerastoderma glaucum, Paphia senescens, Varicorbula gibba*), and freshwater (*Viviparus* sp.) mollusc species in the Surozhian fauna assemblage. However, these sediments can be attributed to the Chernomorian (MIS 1) Epoch. Nevertheless, the waters from the Surozh transgression of the Black Sea may have entered the Kerch Strait's erosional cutout due to the strait's deepening during the post-Karangatian regression (Fig. 11g).

The East European Plain's climate was interstadial (Velichko, 1991; Panin et al., 2017). Multi-proxy records from the SE Black Sea shelf core indicate a steppe landscape and arid climate, revealing warmer conditions in northern Anatolia between 64 and 20 ka BP (Shumilovskikh et al., 2014; Wegwerth et al., 2016). In the Azov region, poorly developed soddy Bryansk soil was formed on the thin Early Valdai (MIS 4) loess (Velichko et al., 2017). This soil's spore-pollen spectrum reflects vegetation's dominance close to modern forb-turf-grass steppes. In the Eltigen section's central part, signs of poorly developed paleosol (possibly Bryansk) no older than 69 ka were also discovered (Table 2, Fig. 5).

5.2.5. Neoeuxinian regression and transgression (MIS 2)

The Bryansk interstadial warming (MIS 3) was replaced by the epoch of maximum global cooling (MIS 2). There was a significant decrease in the level of the World Ocean (Menviel et al., 2019). Various estimates suggest that the Mediterranean Sea coastline could have been at levels of −120 to −150 m (Lambeck and Purcell, 2005; Caruso et al., 2011; Palombo et al., 2017), while the Black Sea level could have dropped to −90 to −120 m (Svitoch, 2008; Dolukhanov and Arslanov, 2009; Yanko-Hombach et al., 2011; Larchenkov and Kadurin, 2011; Yanina, 2012).

Active erosion in the Kerch Strait washed away previously accumulated Quaternary sediments, and an erosion incision reached −70 m

(Shnyukov et al., 1981). The strait was a deep erosional valley of the paleo-Don River with steep western and flatter eastern shores (Fig. 11h). The paleo-Don crossed the bottom of the drained Sea of Azov (Yanina, 2012) and carried its waters and sediments directly into the Black Sea (Blagovolin, 1962). During this time, the strait and adjacent water areas began to take shape as they are today (Blagovolin, 1962; Shnyukov et al., 1981). Alluvial deposits of the Kuban River related to the MIS 2 were not discovered in the Kerch Strait (Shnyukov et al., 1981); apparently, the river's main flow occurred directly into the Black Sea. The main phase of loess accumulation in the Azov region dates back to the time of maximum glaciation; the obtained spore-pollen spectra of loess deposits showed a sharp predominance of grass and shrub pollen (Velichko et al., 2017). The species composition of the flora corresponds to the dry steppe landscapes of the extreme cryo-arid environments. Along the shores of the Kerch Strait, there is a horizon of loess-like loams on poorly developed, presumably Bryansk soil, indicating periglacial climatic conditions (Tables 1 and 2, Fig. 5). The age of a sample from the upper part of the loess-like deposits of the Eltigen section was determined by the OSL method to be ~20 ka (Table 1, Fig. 5), which indicates that the time of its accumulation corresponds to the Last Glacial Maximum. The warming that began after the maximum global cooling and a significant increase in atmospheric precipitation within the East European Plain during ~19–17 and ~15–13 ka BP led to active snow-melt and thawing of permafrost, which in turn caused a significant increase in water supply and runoff (Tudryn et al., 2016; Panin et al., 2017; Sidorchuk et al., 2018; Borisova, 2021). The sharply increased riverine water supply caused rapid Neoeuxinian Black Sea Basin transgression. In the Tuzla Island area, a freshwater estuary/delta formed from the backwater of the paleo-Don, which later became a slightly brackish-water lagoon (Fig. 11i). The shells of brackish-water Caspian molluscs appear in the Kerch Strait (Figs. 9 and 10). They likely entered the Neoeuxinian Basin with the water flow from the early Khvalynian transgressive basin of the Caspian Sea. According to recent geochronological data, the flow was estimated to have occurred 18–13 ka BP (Yanina et al., 2017; Kurbanov et al., 2021; Semikolennykh et al., 2022, 2024; Makshaev and Tkach, 2023).

5.2.6. Chernomorian (Black Sea) transgression (MIS 1)

The penetration of salty Mediterranean waters into the Black Sea basin, resulting from the transgression of the World Ocean, began ~9.4–8.4 ka BP (Ryan et al., 2003; Major et al., 2006; Soulet et al., 2011; Çağatay et al., 2022). Seawater flow into the Kerch Strait also began at the beginning of the Holocene, which is noted in the core of all four boreholes from Tuzla Island by the appearance of the first representatives of the Mediterranean fauna (Table 4, Figs. 9 and 10). The staged entry of Mediterranean waters into the Black Sea Basin and the gradual increase in the salinity of the basin led to the successive colonisation of the Kerch Strait by Mediterranean species of molluscs — from euryhaline to moderately euryhaline and moderately stenohaline. The faunal composition of boreholes' sedimentary successions in Tuzla Island shows an unstable sea level position with fluctuations of different signs at the initial stage of the Black Sea transgression development. The horizons of the boreholes' successions with the largest number of marine stenohaline species in the composition of sediments were dated in the range from 6050 ± 140 to 5590 ± 160 years (Table 4, Fig. 9), which is probably associated with the Holocene Climatic Optimum (Nielsen et al., 2018). This period's highest sea surface salinity (~20 ‰) was also reconstructed between 5.4 and 2.5 cal ka BP in the SE Black Sea shelf (Shumilovskikh et al., 2013a). Large accumulative forms, such as the Tuzla and Chushka spits, have only been formed within the Kerch Strait in the last three thousand years. The current stage of the Kerch Strait development (Fig. 11j) is characterised by the distribution of shells of Mediterranean euryhaline and moderately stenohaline species in the sediments.

6. Conclusion

The Late Pleistocene — Holocene history of the Kerch Strait is a closed cycle (Fig. 11a). This cycle involves the transformation of the classic marine strait into a large riverbed, followed by a freshwater estuary, a brackish lagoon or delta, and then becoming part of a vast drainage channel. Eventually, it transforms back into a marine strait again. All the stages in the development of the Kerch Strait were in response to changing conditions in the Mediterranean—Pont—Caspian system due to global climate change.

During interglacial periods and relatively warm interstadials (e.g. MIS 5e-c and MIS 1), the Sea of Azov and the Black Sea are connected by the Kerch Strait. This connection enables water exchange between the two basins, and marine molluscs inhabit the strait.

Following the regression of the World Ocean and, consequently, the Black Sea (MIS 5b — MIS 2), the basin of the Azov Sea was drained. As a result, the mouth of the Don River shifted to the Black Sea shelf, bypassing the Kerch Strait. The channel is actively incised, and as the sea level rises and the river backs up, the alluvial channel and delta deposits accumulate in the strait.

During the past 130,000 years, the Kerch Strait served as a pathway for the flow of Caspian waters during two periods. This occurred during the transition from interglacial to glacial and from glacial to interglacial epochs. Specifically, these periods were the MIS 5c, when there was a Hyrcanian runoff, and the MIS 2, when there was a Khvalynian runoff.

During the Holocene transgression (MIS 1) of the World Ocean, which followed the pattern of the Eemian transgression (MIS 5e), the Kerch Strait once again became a marine strait. As a result, the strait was repopulated by marine fauna.

Author contributions

The author (Daria Semikolennykh) confirms sole responsibility for the following: study conception and design, data collection, analysis and interpretation of results, and manuscript preparation.

Declaration of competing interest

The authors declare that they have no known competing financial interests or personal relationships that could have appeared to influence the work reported in this paper.

Data availability

Data will be made available on request.

Acknowledgements

Appendix A. Supplementary data

Supplementary data to this article can be found online at https://doi.org/10.1016/j.quascirev.2024.108914.

References

Afanasenkov, A.P., Nikishin, A.M., Obukhov, A.N., 2007. Geological Structure and Hydrocarbon Potential of the East Black Sea Region. Nauchny mir, Moscow, p. 172 in Russian.

Andrusov, N.I., 1903. Geological studies on the taman peninsula. Materialy dlya geologii Rossii XXI (2), 257–283 in Russian.

Andrusov, N.I., 1904. On the age of the marine post-Tertiary terraces of the Kerch Peninsula. Ezhegodnik po Geologii i Mineral. Rossii 7 (6), 158–172 in Russian.

Andrusov, N.I., 1918. Geological structure of the Kerch Strait bottom. Izv. AN SSSR. Ser. 6 12 (1), 23–28 in Russian.

Arkhangelsky, A.D., Strakhov, N.M., 1938. Geological Structure and History of Development of the Black Sea. Publishing House of Academy of Sciences of the USSR, Moscow-Leningrad in Russian.

Arslanov, Kh.A., Gerasimova, S.A., Izmailov, YaA., Lokshin, N.V., Muratov, V.M., Ostrovsky, A.B., Tyrtychnyi, N.I., Scheglov, A.P., 1972. On the age of the Holocene and upper Pleistocene deposits of the Black Sea coast of the Caucasus and the Kerch-Taman region. Nauchnie Novosti i Zametki 107–110 in Russian.

Arslanov, Kh.A., Balabanov, I.P., Gey, N.A., 1983. About age and climatic conditions of formation of sediments of the late Pleistocene marine terraces of the coast of the Kerch Strait. Vestn. Leningr. Univers 12, 69–79 in Russian.

Autzen, M., Andersen, C.E., Bailey, M., Murray, A.S., 2022. Calibration quartz: an update on dose calculations for luminescence dating. Radiat. Meas. 157, 106828 https://doi.org/10.1016/j.radmeas.2022.106828.

Badertscher, S., Fleitmann, D., Cheng, H., Edwards, R.L., Göktürk, O.M., Zumbühl, A., Leuenberger, M., Tüysüz, O., 2011. Pleistocene water intrusions from the Mediterranean and Caspian seas into the Black Sea. Nature Geosci 4, 236–239. https://doi.org/10.1038/ngeo1106.

Bagriy, I.D., Pochtarenko, V.I., Aksyom, S.D., Shekhunova, S.B., Znamenskaya, T.A., Maslun, N.V., Dubosarsky, V.R., Kravchinsky, R.L., Yantsevich, A.A., 2008. Features of lithodynamic processes and material composition of bottom sediments in the coastal part of the Tuzla Spit. Geologist of Ukraine 1–2, 99–110 in Russian.

Balabanov, I.P., Izmailov, Y.A., 1988. Change of level and hydrochemical mode of the Black and Azov seas for the last 20 thousand years. Water Resour. (6), 54–63 in Russian.

Ballesteros, D., Rodríguez-Rodríguez, L., González-Lemos, S., Giralt, S., Álvarez-Lao, D., Adrados, L., Jiménez-Sánchez, M., 2017. New evidence of sea-level lowstands and paleoenvironment during MIS 6 and 4 in the Cantabrian coastal karst: the Cobiheru cave (North Iberia). Earth Surf. Process. Landforms 42 (11), 1704–1716. https://doi.org/10.1002/esp.4115.

Baskakova, G.V., Nikishin, A.M., 2018. History of the formation of the Kerch-Taman zone region based on the reconstruction of a balanced regional section. 2018. Bulletin of Moscow University. Ser. 4: Geology 23–29 in Russian.

Benjamin, J., Rovere, A., Fontana, A., Furlani, S., Vacchi, M., Inglis, R.H., Galili, E., Antonioli, F., Sivan, D., Miko, S., Mourtzas, N., Felja, I., Meredith-Williams, M., Goodman-Tchernov, B., Kolaiti, E., Anzidei, M., Gehrels, R., 2017. Late Quaternary sea-level changes and early human societies in the central and eastern Mediterranean Basin: an interdisciplinary review. Quat. Int. 449, 29–57. https://doi.org/10.1016/j.quaint.2017.06.025.

Berndt, Ch, Frenzel, P., Çiner, A., Ertunç, G., Yıldırım, C., 2019. Holocene marginal marine ostracod successions from the Kızılırmak River delta; Implications for depositional environments and sea-level changes at the Southern Black Sea coast. Sediment. Geol. 382, 103–121. https://doi.org/10.1016/j.sedgeo.2019.01.013.

Blagovolin, N.S., 1960. Origin and history of the evolution of the Kerch Strait. Izv. Akademii nauk SSSR. Ser. geomorph. No 2, 105–109 in Russian.

Blagovolin, N.S., 1962. Geomorphology of the Kerch-Taman Zone. Akad. Nauk SSSR, Moscow, p. 201 in Russian.

Borisova, O.K., 2021. Landscape and climatic conditions in the central East European Plain in the last 22 thousand years: reconstruction based on paleobotanical data. Water Resour. 48 (6), 886–896. https://doi.org/10.1134/S0097807821060038.

Bøtter-Jensen, L., Bulur, E., Duller, G.A.T., Murray, A.S., 2000. Advances in luminescence instrument systems. Radiat. Meas. 32, 523–528. https://doi.org/10.1016/S1350-4487(00)00039-1.

Bøtter-Jensen, L., Bulur, E., Murray, A.S., Poolton, N.R., 2002. Enhancements in luminescence measurement techniques. Radiat. Protect. Dosim. 101 (No 1–4), 119–124. https://doi.org/10.1093/oxfordjournals.rpd.a005950.

Bronk Ramsey, C., Lee, S., 2013. Recent and planned developments of the program OxCal. Radiocarbon 55 (No 2–3), 720–730. https://doi.org/10.1017/S0033822200057878.

Buylaert, J.-P., Jain, M., Murray, A.S., Thomsen, K.J., Thiel, C., Sohbati, R., 2012. A robust feldspar luminescence dating method for Middle and Late Pleistocene sediments. Boreas 41 (3), 435–451. https://doi.org/10.1111/j.1502-3885.2012.00248.x.

Büyükmeriç, Y., Wesselingh, F., Alçiçek, M., 2016. Middle-late Pleistocene marine molluscs from the Izmit Bay area (eastern Marmara Sea, Turkey) and the nature of Marmara — black Sea corridors. Quat. Int. 401, 153–161. https://doi.org/10.1016/j.quaint.2015.07.020.

Çağatay, M.N., Eriş, K., Ryan, W.B.F., Sancar, Ü., Polonia, A., Akçer, S., Biltekin, D., Gasperini, L., Görür, N., Lericolais, G., Bard, E., 2009. Late pleistocene–holocene evolution of the northern shelf of the Sea of Marmara. Mar. Geol. V. 265 (No 3–4), 81–100. https://doi.org/10.1016/j.margeo.2009.06.011.

Çağatay, M.N., Eriş, K.K., Makaroglu, O., Yakupoglu, N., Henry, P., Leroy, S.A.G., Uçarkus, G., Sakınç, M., Yalamaz, B., Bozyigit, C., Kende, J., 2019. The Sea of Marmara during marine isotope stages 5 and 6. Quat. Sci. Rev. 220, 124–141. https://doi.org/10.1016/j.quascirev.2019.07.031.

Çağatay, M.N., Eriş, K.K., Erdem, Z., 2022. Morphology and Late Pleistocene–Holocene Sedimentation of the Strait of Istanbul (Bosphorus): a Review, vol. 523. Geological Society, London, Special Publications, pp. 213–228. https://doi.org/10.1144/sp523-2021-48.

Caruso, A., Cosentino, C., Pierre, C., Sulli, A., 2011. Sea-level change during the last 41 ka in the other shelf of southern Tyrrhenian Sea. Quat. Int. 232, 137–149. https://doi.org/10.1016/j.quaint.2010.07.034.

Chepalyga, A.L., 2002. The Black Sea. In: Velichko, A.A. (Ed.), Dynamics of Landscape Components and Internal Sea Basins of the Northern Eurasia for the Last 130000 Years. GEOS Publ, Moscow, pp. 170–182 in Russian.

Chepalyga, A.L., 2006. Epoch of extreme floodings in an arid zone of Northern Eurasia. Late Cainozoic geological history of the north of the arid zone. Rostov-on-Don 166–171 in Russian.

Cresswell, A.J., Carter, J., Sanderson, D.C.W., 2018. Dose rate conversion parameters: assessment of nuclear data. Radiat. Meas. 120, 195–201. https://doi.org/10.1016/j.radmeas.2018.02.007.

Cunningham, A.C., Buylaert, J.-P., Murray, A.S., 2022. Attenuation of beta radiation in granular matrices: implications for trapped-charge dating. Geochronology 4, 517–531. https://doi.org/10.5194/gchron-4-517-2022.

Dodonov, A.E., Tchepalyga, A.L., Mihailescu, C.D., Zhou, L.P., Markova, A.K., Trubikhin, V.M., Simakova, A.N., Konikov, E.G., 2000. Last-interglacial records from central Asia to the northern Black Sea shoreline: stratigraphy and correlation. Neth. J. Geosci. 79 (No 2–3), 303–311. https://doi.org/10.1017/S0016774600021788.

Dolukhanov, P.M., Arslanov, H.A., 2009. Ecological crises and early human migration in the Black Sea area. Quat. Int. 197, 35–42. https://doi.org/10.1016/j.quaint.2007.08.035.

Dutton, A., Carlson, A.E., Long, A.J., Milne, G.A., Clark, P.U., DeConto, R., Horton, B.P., Rahmstorf, S., Raymo, M.E., 2015. Sea-level rise due to polar ice-sheet mass loss during past warm periods. Science 349, 4019. https://doi.org/10.1126/science.aaa401.

Eberzin, A.G., 1935. About the chauda layers of the Taman Peninsula. Dokl. AN SSSR 2 (No 8–9), 580–587 in Russian.

Erginal, A.E., Kıyak, N.G., Makaroglu, O., Bozcu, M., Öztürk, M.Z., Selim, H.H., Nowaczyk, N.R., Kaya, N., Ozturk, T., Karabıyıkoglu, M., Polymeris, G.S., 2022. Aeolian imprints of multiple mediterranean invasions of the Black Sea during Pleistocene. Palaeogeogr. Palaeoclimatol. Palaeoecol. 592, 110902 https://doi.org/10.1016/j.palaeo.2022.1109.

Fedorov, P.V., 1963. Stratigraphy of the Quaternary Deposits of the Crimean-Caucasian Coast and Some Questions of the Geological History of the Black Sea. AN SSSR Publ, Moscow, p. 164 in Russian.

Fedorov, P.V., 1978. The Ponto-Caspian Pleistocene. Nauka Publ, Moscow, p. 165 in Russian.

Gaydalenok, O.V., Shmatkov, A.A., Shmatkova, A.A., Olkhovsky, S.V., 2019. Results of ultra-high-resolution seismoacoustic survey offshore Taman Bay in the area of the ancient city of Phanagoria. Izv. Atmos. Ocean. Phys 55 (11), 1749–1754. https://doi.org/10.1134/S0001433819110021.

Gzam, M., El Mejdoub, N., Jedoui, Y., 2016. Late quaternary sea-level changes of Gabes coastal plain and shelf: identification of the MIS 5c and MIS 5a onshore highstands, southern Mediterranean. Earth Syst. Sci. 125, 13–28. https://doi.org/10.1007/s12040-015-0649-7.

Hoyle, T.M., Bista, D., Flecker, R., Krijgsman, W., Sangiorgi, F., 2021. Climate-driven connectivity changes of the Black Sea since 430 ka: testing a dual palynological and geochemical approach. Palaeogeogr. Palaeoclimatol. Palaeoecol. 561, 110069 https://doi.org/10.1016/j.palaeo.2020.110069.

Ignatov, E.I., Chistov, S.V., 2003. Ecological and geomorphological assessment of the coast and bottom of the Kerch Strait in connection with solving transport problems. Environmental safety of coastal and shelf zones and integrated use of shelf resources. Sevastopol: NAN Ukrainy 8, 163–174 in Russian.

Kaytamba, M.D., 2005. Vegetation in the Late Pleistocene and Holocene. Abstract of Ph. D. thesis: 25.00.25. Moscow. 182 pp. in Russian.

Khain, V.E., Popkov, V.I., 2009. Tectonics of Southern Framing of the East European Craton. Krasnodar, p. 213 in Russian.

Krijgsman, W., Tesakov, A., Yanina, T., Lazarev, S., Danukalova, G., Van Baak, C.G.C., Agustí, J., Alçiçek, M.C., Aliyeva, E., Bista, D., Bruch, A.A., Büyükmeriç, Y., Bukhsianidze, M., Flecker, R., Frolov, P., Hoyle, T.M., Jorissen, E.L., Kirscher, U., Koriche, S.A., Kroonenberg, S.B., Lordkipanidze, D., Oms, O., Rausch, L., Singarayer, J., Stoica, M., Van de Velde, S., Titov, V.V., Wesselingh, F.P., 2019. Quaternary time scales for the Pontocaspian domain: interbasinal connectivity and faunal evolution. Earth Sci. Rev. 188, 1–40. https://doi.org/10.1016/j.earscirev.2018.10.013.

Kurbanov, R.N., Yanina, T.A., Murray, A.S., Borisova, O.K., 2018. Hyrkanian stage in the late Pleistocene history of the Manych depression. Vestn. Mosk. un-ta. Ser. 5. Geogr (3), 77–88 in Russian.

Kurbanov, R.N., Yanina, T.A., Murray, A.S., Semikolennykh, D.V., Svistunov, M.I., Shtyrkova, E.I., 2019. The age of the karangatian (late Pleistocene) transgression of the Black Sea. Vestn. Mosk. Univ. Seriya 5 Geogr. (6), 29–39 in Russian.

Kurbanov, R.N., Semikolennykh, D.V., Yanina, T.A., Tyunin, N.A., Murray, A.S., 2020. New data on the age of the Karangatian transgression of the Black Sea. Vestn. Mosk. Univ. Seriya 5 Geogr. (6), 139–145 in Russian.

Kurbanov, R.N., Murray, A.S., Thompson, W., Svistunov, M.I., Taratunina, N.A., Yanina, T.A., 2021. First reliable chronology for the early khvalynian Caspian Sea transgression in the lower Volga river valley. Boreas 50 (1), 134–146. https://doi.org/10.1111/bor.12478.

Kwiecien, O., Arz, H.W., Lamy, F., Wulf, S., Bahr, A., Röhl, U., Haug, G.H., 2008. Estimated reservoir ages of the Black Sea since the last glacial. Radiocarbon 50 (1), 99–118. https://doi.org/10.1017/S0033822200043393.

Lambeck, K., Purcell, A., 2005. Sea-level change in the Mediterranean Sea since the LGM: model predictions for tectonically stable areas. Quat. Sci. Rev. 24, 1969–1988. https://doi.org/10.1016/j.quascirev.2004.06.025.

Larchenkov, E., Kadurin, S., 2011. Paleogeography of the pontic lowland and northwestern Black Sea shelf for the past 25 ky. Geology and geoarchaeology of the Black Sea region: beyond the flood hypothesis. Geological Society of America 473, 71–88. https://doi.org/10.1130/2011.2473(06.

Lisiecki, L.E., Stern, J.V., 2016. Regional and global benthic d18O stacks for the last glacial cycle. Paleoceanography 31, 1–27. https://doi.org/10.1002/2016PA003002.

Lowe, J.J., Walker, M., 2015. Reconstructing Quaternary Environments, third ed. Routledge, London, p. 539. https://doi.org/10.4324/9781315797496.

Major, C.O., Goldstein, S.L., Ryan, W.B., Lericolais, G., Piotrowski, A.M., Hajdas, I., 2006. The co-evolution of Black Sea level and composition through the last deglaciation and its paleoclimatic significance. Quat. Sci. Rev. 25, 2031–2047. https://doi.org/10.1016/j.quascirev.2006.01.032.

Makshaev, R.R., Tkach, N.T., 2023. Chronology of Khvalynian stage of the Caspian Sea according to radiocarbon dating. Geomorfologiya i Paleogeografiya 54 (1), 37–54. https://doi.org/10.31857/S0435428123010108 in Russian.

Markova, A.K., 2000. The Mikulino (=Eemian) mammal faunas of the Russian plain and crimea. Geol. Mijnbouw 79 (2), 293–301.

Marra, F., Rolfo, M.F., Gaeta, M., Florindo, F., 2020. Anomalous last interglacial tyrrhenian sea levels and neanderthal settling at guattari and moscerini caves (central Italy). Sci. Rep. 10, 11929 https://doi.org/10.1038/s41598-020-68604-z.

Menviel, L., Capron, E., Govin, A., Dutton, A., Tarasov, L., Abe-Ouchi, A., Drysdale, R.N., Gibbard, P.L., Gregoire, L., He, F., Ivanovic, R.F., Kageyama, M., Kawamura, K., Landais, A., Otto-Bliesner, B.L., Oyabu, I., Tzedakis, P.C., Wolff, E., Zhang, X., 2019. The penultimate deglaciation: protocol for Paleoclimate Modelling Intercomparison Project (PMIP) phase 4 transient numerical simulations between 140 and 127 ka, version 1.0. Geosci. Model Dev. (GMD) 12, 3649–3685. https://doi.org/10.5194/gmd-12-3649-2019.

Mikhailov, V.N., Magritsky, D.V., Ivanov, A.A., 2010. Hydrology of Delta and Seashore Estuary of the Kuban River. GEOS (Publ.), Moscow, p. 728 in Russian.

Murray, A.S., Wintle, A.G., 2000. Luminescence dating of quartz using an improved single-aliquot regenerative-dose protocol. Radiat. Meas. 32 (1), 57–73. https://doi.org/10.1016/S1350-4487(99)00253-X.

Murray, A.S., Wintle, A.G., 2003. The single aliquot regenerative dose protocol: potential for improvements in reliability. Radiat. Meas. 37, 377–381. https://doi.org/10.1016/S1350-4487(03)00053-2.

Murray, A., Marten, R., Johnston, A., Martin, P., 1987. Analysis for naturally occurring radionuclides at environmental concentrations by gamma spectrometry. J. Radioanal. Nucl. Chem. 115, 263–288. https://doi.org/10.1007/BF02037443.

Murray, A.S., Helsted, L.M., Jain, M., Buylaert, J.-P., 2018. Measurement of natural radioactivity: calibration and performance of a high-resolution gamma spectrometry facility. Radiat. Meas. V. 120, 215–220. https://doi.org/10.1016/j.radmeas.2018.04.006.

Murray, A.S., Buylaert, J.-P., Guérin, G., Qin, J., Singhvi, A.K., Smedley, R.S., Thomsen, K.J., 2021. Optically stimulated luminescence dating using quartz sand. Nature Reviews Methods Primers 1, 72. https://doi.org/10.1038/s43586-021-00068-5.

Nevesskaya, L.A., 1965. Late Quaternary Molluscs of the Black Sea, Their Systematisation and Ecology. Academy of Sciences of the USSR publ, Moscow, p. 392 in Russian.

Nevesskaya, L.A., 2007. History of the genus didacna (Bivalvia: cardiidae). Paleontol. J. V. 41, 861–949. https://doi.org/10.1134/S0031030107090018.

Nevesskaya, L.A., Nevessky, E.N., 1961. On the relationship between the Karangatian and Neo-Euxinian layers in the coastal areas of the Black Sea. Reports of the Academy of Sciences of the USSR 136 (5), 256–261 in Russian.

Nielsen, L.T., Aðalgeirsdóttir, G., Vasileios Gkinis, V., Nuterman, R., Hvidberg, Ch.S., 2018. The effect of a Holocene climatic optimum on the evolution of the Greenland ice sheet during the last 10 kyr. J. Glaciol. 64 (245), 477–488. https://doi.org/10.1017/jog.2018.40.

Palombo, M.R., Antonioli, F., Lo Presti, V., Mannino, M., Melis, M.R., Orrù, P., Stocchi, P., Talamo, S., Quarta, G., Calcagnile, L., Deiana, G., Altamura, S., 2017. The Late Pleistocene to Holocene palaeogeographic evolution of the Porto Conte area: clues for a better understanding of human colonization of Sardinia and faunal dynamics during the last 30 ka. Quat. Int. No 439 (Part A), 117–140. https://doi.org/10.1016/j.quaint.2016.06.014.

Panin, A., Grzegorz, A., Buylaert, J.-P., Matlakhova, E., Moska, P., Novenko, E., 2017. Two Late Pleistocene climate-driven incision/aggradation rhythms in the middle Dnieper River basin, west-central Russian Plain. Quat. Sci. Rev. 166, 266–288. https://doi.org/10.1016/j.quascirev.2016.12.002.

Pasynkov, A.A., 2005. On the issue of lithodynamic processes in the Kerch Strait and the area of the Tuzla spit island. Geology and minerals of the World Ocean 2, 120–126 in Russian.

Peshkov, V.M., Porotov, A.V., Gusakov, I.N., 2005. On the issue of restoring the Tuzla Spit. Geol. and floor. fossil World ocean (2), 127–135 in Russian.

Pilipenko, O.V., Trubikhin, V.M., 2012. Geological and paleomagnetic correlation of the Pleistocene sections of the south of Russia, Ukraine and Azerbaijan. Bulletin of the Commission on Studying the Quaternary Period (72), 136–148 in Russian.

Pilipenko, O.V., Trubikhin, V.M., 2015. Paleomagnetic studies of upper neopleistocene rocks from the el'tigen cross section, Kerch peninsula. Geomagn. Aeron. 55 (6), 821–829. https://doi.org/10.1134/S0016793215060110.

Pilipenko, O.V., Abrahamsen, N., Trubikhin, V.M., 2007. Recording of the geomagnetic field from sedimentary deposits of the Tuzla section (Krasnodar region) in the time interval of 120–70 thousand years. Physics of the Earth (8), 74–84 in Russian.

Polyak, V.J., Onac, B.P., Fornós, J.J., Hay, C., Asmerom, Ye, Dorale, J.A., Ginés, J., Tuccimei, P., Ginés, A., 2018. A highly resolved record of relative sea level in the

western Mediterranean Sea during the last interglacial period. Nature Geosci 11, 860–864. https://doi.org/10.1038/s41561-018-0222-5.

Popov, G.I., 1983. Pleistocene of the Black Sea and Caspian Sea Passages. Nauka Publ, Moscow, p. 216 in Russian.

Pravoslavlev, P.A., 1928. Conditions of occurrence of post-Tertiary shell rocks of the Azov and Black seas. Tr. Geol. muzeya AN SSSR 4, 119–196 in Russian.

Prescott, J.R., Hutton, J.T., 1994. Cosmic ray contributions to dose rates for luminescence and ESR dating: large depths and long-term time variations. Radiat. Meas. V. 23 (2–3), 497–500. https://doi.org/10.1016/1350-4487(94)90086-8.

Reimer, P., Austin, W., Bard, E., Bayliss, A., Blackwell, P., Bronk Ramsey, C., Butzin, M., Cheng, H., Edwards, R., Friedrich, M., Grootes, P., Guilderson, T., Hajdas, I., Heaton, T., Hogg, A., Hughen, K., Kromer, B., Manning, S., Muscheler, R., Palmer, J., Pearson, C., van der Plicht, J., Reimer, R., Richards, D., Scott, E., Southon, J., Turney, C., Wacker, L., Adolphi, F., Büntgen, U., Capano, M., Fahrni, S., Fogtmann-Schulz, A., Friedrich, R., Köhler, P., Kudsk, S., Miyake, F., Olsen, J., Reinig, F., Sakamoto, M., Sookdeo, A., Talamo, S., 2020. The IntCal20 Northern Hemisphere radiocarbon age calibration curve (0–55 cal kBP). Radiocarbon 62 (4), 725–757. https://doi.org/10.1017/RDC.2020.41.

Rogozhin, E.A., Gorbatikov, A.V., Ovsyuchenko, A.N., 2015. Active faults and deep structure of the Kerch Strait zone. Geology and geophysics of the South of Russia 1, 65–68 in Russian.

Ryan, W.B.F., Major, C.O., Lericolais, G., Goldstein, S.L., 2003. Catastrophic flooding of the Black Sea. Annual Reviews of Earth and Planetary Sciences 31, 525–554. https://doi.org/10.1146/annurev.earth.31.100901.141249.

Salonen, J.S., Helmens, K.F., Brendryen, J., Kuosmanen, N., Väliranta, M., Goring, S., Korpela, M., Kylander, M., Philip, A., Plikk, A., Renssen, H., Luoto, M., 2018. Abrupt high-latitude climate events and decoupled seasonal trends during the Eemian. Nat. Commun. 9, 2851. https://doi.org/10.1038/s41467-018-05314-1.

Semenenko, V.N., Kovaluykh, N.N., 1973. Absolute age of the Upper Quaternary deposits of the Azov-Black Sea basin according to the data of radiocarbon analysis. Geol. Zh. (Kiev. 1968) V. 33 (No 6), 91–97 in Russian.

Semenenko, V.N., Sidenko, O.G., 1979. Reflection of deep structures in marine Quaternary sediments of the central part of the Azov Sea. Late Quaternary history and sedimentogenesis of marginal and inland seas. Moscow: Nauka 87–99 in Russian.

Semikolennykh, D., Arslanov, Kh, Ignatov, Eu, Luksha, V., 2018. Evolution of the natural environment of the Kerch strait area during recent 25 thousand years. Vestn. Mosk. Univ. Seriya 5 Geogr. (5), 55–61 in Russian.

Semikolennykh, D.V., Kurbanov, R.N., Yanina, T.A., 2022. Age of the Khvalynian Strait in the Late Pleistocene History of the Manych Depression. Vestnik Moskovskogo Universiteta Ser. 5. Geografiya 5, 103–112 in Russian.

Semikolennykh, D.V., Kurbanov, R.N., Yanina, T.A., 2023a. Chronology of the Karangatian transgression of the Black Sea by luminescence dating. Izvestia RAS. Seria geograficheskaya. V. 87 (1), 88–101 in Russian.

Semikolennykh D.V., Kurbanov R.N., Yanina T.A., 2023b. Ingression of the Karangatian Sea into the Manych Depression (Late Pleistocene). Vestnik Moskovskogo Universiteta. Ser. 5. Geografiya. No 6. P. 96–106. in Russian.

Semikolennykh, D., Panin, A., Zazovskaya, E., 2024. Radiocarbon dating of the end of the latest Caspian Sea overflow through the Manych Depression (Southeastern European Plain). Radiocarbon. Preprint.

Shelkoplyas, V.N., Khristoforova, T.F., 2007. On the structure of marine Quaternary deposits of the Kerch region. Geology and Minerals of the World Ocean 2, 120–126 in Russian.

Shii, Ch, Rostovtseva, Y.U.V., 2013. Feeding provinces of the Kerch-Taman trough in the pliocene and Pleistocene. Vestnik Moskovskogo universiteta. Seriya 4: Geologiya (4), 51–55 in Russian.

Shnyukov, E.F., Alenkin, V.M., Inozemtsev, Yu.I., Naumenko, P.I., Put, A.L., Skiba, S.I., 1981. Geology of the Shelf of the Ukrainian SSR. Kerch Strait. Naukova Dumka, Kiev, p. 160 in Russian.

Shnyukov, E.F., Sobolevskij, YuV., Gnatenko, G.I., Naumenko, P.I., Kutnij, V.A., 1986. Mud Volcanoes of the Kerch-Taman Region: Atlas. Naukova dumka, Kiev, p. 152. In Russian.

Shumilovskikh, L.S., Marret, F., Fleitmann, D., Arz, H.W., Nowaczyk, N., Behling, H., 2013a. Eemian and Holocene sea-surface conditions in the southern Black Sea: organic-walled dinoflagellate cyst record from core 22-GC3. Mar. Micropaleontol. 101, 146–160. https://doi.org/10.1016/j.marmicro.2013.02.001.

Shumilovskikh, L.S., Arz, H.W., Wegwerth, A., Fleitmann, D., Marret, F., Nowaczyk, N., Tarasov, P., Behling, H., 2013b. Vegetation and environmental changes in northern Anatolia between 134 and 119 ka recorded in Black Sea sediments. Quat. Res. 80 (3), 349–360. https://doi:10.1016/j.yqres.2013.07.005.

Shumilovskikh, L.S., Fleitmann, D., Nowaczyk, N., Behling, H., Marret, F., Wegwerth, A., Arz, H.W., 2014. Orbital and millennial-scale environmental variability during 64–25 ka BP as detected in pollen and dinocyst records from the SE Black Sea. Clim. Past Discuss (9), 5439–5477. https://doi.org/10.5194/cp-10-939-2014.

Siani, G., Paterne, M., Arnold, M., Bard, E., Métivier, B., Nadine, Tisnerat N., Bassinot, F., 2016. Radiocarbon reservoir ages in the Mediterranean Sea and Black Sea. Radiocarbon 42 (No 2), 271–280. https://doi:10.1017/S0033822200059075.

Sidorchuk, A.Yu, Panin, A.V., Borisova, O.K., 2018. River flow on the East European Plain over the last 20 thousand years and the problem of changes in levels of the southern seas. Questions of geography 145, 144–168 in Russian.

Simonov, D.A., Bryantseva, G.V., 2018. Morphostructural analysis during neotectonic reconstructions of the Kerch Peninsula. Byull. MOIP. Otd. Geol 93, 12–25 in Russian.

Sivan, D., Sisma-Ventura, G., Greenbaum, N., Bialik, O.M., Williams, F.H., Tamisiea, M. E., Rohling, E.J., Frumkin, A., Avnaim-Katav, S., Shtienberg, G., Stein, M., 2016. Eastern Mediterranean Sea levels through the last interglacial from a coastal marine

sequence in northern Israel. Quat. Sci. Rev. 145, 204–225. https://doi.org/10.1016/j.quascirev.2016.06.001.

Sorokin, V.M., 2011. Correlation of upper Quaternary deposits and palaeogeography of the Black and Caspian seas. Stratigr. Geol. Correl. 19 (5), 563–578. https://doi.org/10.1134/S086959381104006X.

Soulet, G., Ménot, G., Lericolais, G., Bard, E., 2011. A revised calendar age for the last reconnection of the Black Sea to the global ocean. Quat. Sci. Rev. 30, 1019–1026. https://doi.org/10.1016/j.quascirev.2011.03.001.

Spratt, R.M., Lisiecki, L.E., 2016. A Late Pleistocene sea level stack. Clim. Past 12, 1079–1092. https://doi.org/10.5194/cp-12-1079-2016.

Svitoch, A.A., 2008. The khvalynian transgression of the Caspian Sea and the new-euxinian Basin of the Black Sea. Water Resour. 35 (2), 165–170. https://doi.org/10.1134/S0097807808020048.

Svitoch, A.A., 2009. Karangatian stratotypes of the taman and Kerch peninsulas (comparative analysis). Dokl. Akad. Nauk 424, 669–671 in Russian.

Svitoch, A.A., Makshaev, R.R., 2017. The interconnectivity of palaeogeographic events within the Pont-Manych-Caspian system during the late Pleistocene and the Holocene. Vestn. Mosk. Univ. Seriya 5 Geogr. (2), 24–32 in Russian.

Svitoch, A.A., Novichkova, T.S., 2001. Lithology and sedimentation conditions of the chaudin deposits of the taman peninsula (reference sections pekla and Tuzla). Lithology and minerals 5, 547–553 in Russian.

Svitoch, A.A., Blyum, N.S., Bolikhovskaya, N.S., Taldenkova, E.E., Yanina, T.A., Markova, A.K., Polyakova, E.I., Sudakova, N.G., Nikolaev, S.D., Faustov, S.S., Glushankova, N.I., 1999. Methods for Diagnostics and Correlation of Paleogeographic Events. Mosk. Gos. Univ., Moscow, p. 348 in Russian.

Trikhunkov, YaI., Bachmanov, D.M., Gaydalenok, O.V., Marinin, A.V., Sokolov, S.A., 2019. Recent Mountain-building at the boundary juction of the north-western Caucasus and intermediate kerch-taman region, Russia. Geotektonika 4, 78–99. https://doi.org/10.31857/S0016-853X2019378-96inRussian.

Tudryn, A., Leroy, S.A.G., Toucanne, S., Gibert-Brunet, E., Tucholka, P., Lavrushin, YuA., Dufaure, O., Miska, S., Bayon, G., 2016. The Ponto-Caspian basin as a final trap for southeastern Scandinavian Ice-Sheet meltwater. Quat. Sci. Rev. 148, 29–43. https://doi.org/10.1016/j.quascirev.2016.06.019.

Tzedakis, P.C., Drysdale, R.N., Margari, V., Skinner, L.C., Menviel, L., Rhodes, R.H., Taschetto, A.S., Hodell, D.A., Crowhurst, S.J., Hellstrom, J.C., Fallick, A.E., Grimalt, J.O., McManus, J.F., Martrat, B., Mokeddem, Z., Parrenin, F., Regattieri, E., Roe, K., Zanchetta, G., 2018. Enhanced climate instability in the north atlantic and southern europe during the last interglacial. Nat. Commun. 9, 4235. https://doi.org/10.1038/s41467-018-06683-3.

Velichko, A.A., 1991. Correlation of late Pleistocene events in glacial regions of the northern hemisphere. Bulletin of the Commission on Studying the Quaternary Period 60, 14–28 in Russian.

Velichko, A.A., Morozova, T.D., Borisova, O.K., Timireva, S.N., Semenov, V.V., Kononov, YuM., Titov, V.V., Tesakov, A.S., Konstantinov, E.A., Kurbanov, R.N., 2012. Formation of the steppe zone in the south of Russia (based on materials of the structure of the loess-soil formation of the Don-Azov region). Reports of the Academy of Sciences 445 (4), 464–467 in Russian.

Velichko, A.A., Borisova, O.K., Zakharov, A.L., Kononov, YuM., Konstantinov, E.A., Kurbanov, R.N., Morozova, T.D., Panin, P.G., Timireva, S.N., 2017. Change of Landscape Conditions in the South of the Russian Plain in the Late Pleistocene According to the Results of a Study of the Loess-Soil Series of the Azov Region, vol. 1. Izvestia RAS. Seria geograficheskaya, pp. 74–83 in Russian.

Wegwerth, A., Dellwig, O., Kaiser, J., Ménot, G., Bard, E., Shumilovskikh, L., Schnetger, B., Kleinhanns, I.C., Wille, M., Arz, H.W., 2014. Meltwater events and the mediterranean reconnection at the saalian–eemian transition in the Black Sea. Earth Planet Sci. Lett. 404, 124–135. https://doi.org/10.1016/j.epsl.2014.07.030.

Wegwerth, A., Kaiser, J., Dellwig, O., Shumilovskikh, L.S., Nowaczyk, N.R., Arz, H.W., 2016. Northern hemisphere climate control on the environmental dynamics in the glacial Black Sea "Lake". Quat. Sci. Rev. 135, 41–53. https://doi.org/10.1016/j.quascirev.2016.01.016.

Wegwerth, A., Dellwig, O., Sabine, Wulf S., Plessen, B., Ilka, C., Kleinhanns, I.C., Norbert, R., Nowaczyk, N.R., Jiabo, L., Arz, H.W., 2019. Major hydrological shifts in the Black Sea "Lake" in response to ice sheet collapses during MIS 6 (130–184 ka BP). Quat. Sci. Rev. 219, 126–144. https://doi.org/10.1016/j.quascirev.2019.07.008.

Yanina, T.A., 2005. Didacna of the Ponto-Caspian. Madzhenta Publ, Moscow, Smolensk, p. 300 in Russian.

Yanina, T.A., 2012. Neo-Pleistocene of the Ponto-Caspian: Biostratigraphy, Palaeogeography, Correlation. MGU, Moscow, p. 264 in Russian.

Yanina, T.A., 2014. The Ponto-Caspian region: environmental consequences of climate change during the late Pleistocene. Quat. Int. 345, 88–99. https://doi.org/10.1016/j.quaint.2014.01.045.

Yanina, T.A., 2020. Environmental variability of the ponto-caspian and mediterranean basins during the last climatic macrocycle. Geography, Environment, Sustainability 13 (No 4), 6–23. https://doi.org/10.24057/2071-9388-2020-120.

Yanina, T.A., Sorokin, V.M., 2022. Surozh transgression in the Late Pleistocene history of the Black Sea (biostratigraphic analysis of drilling materials). PALEOSTRAT-2022. Annual meeting (scientific conference) of the palaeontology section of the MOIP and the Moscow branch of the Paleontological Society of the Russian Academy of Sciences. Moscow: PIN RAS. 74–74 in Russian.

Yanina, T.A., Svitoch, A.A., Kurbanov, R.N., Murray, A.S., Tkach, N.T., Sychev, N.V., 2017. Paleogeographic analysis of the results of optically stimulated luminescence dating of Pleistocene deposits of the Lower Volga area. Vestn. Mosk. Univ. Seriya 5 Geogr. (1), 20–28 in Russian.

Yanina, T., Sorokin, V., Bolikhovskaya, N., Semikolennykh, D., Makshaev, R., Matlakhova, E., 2024. Caspian – black Sea connection during MIS 5 (late

Pleistocene): evidences from integrated analysis of drilling materials. Conference MedGU-2023 Proceedings. Preprint.

Yanko, V.V., Frolov, V.T., Motnenko, I.V., 1990. Foraminifera and lithology of the stratotype horizon (Anthropogene of the Kerch peninsula). Bulletin of the Moscow Society of investigators of the nature. Geology (65), 83–97 in Russian.

Yanko-Hombach, V.V., Smyntyna, E.V., Kadurin, S.V., Larchenkov, E.P., Motnenko, I.V., Kakaranza, S.V., 2011. Fluctuations in the Black Sea level and the adaptation strategy of ancient man over the past 30 thousand years. Geology and minerals of the World Ocean. No 2, 61–94 in Russian.

Zimmerman, D.W., 1971. Thermoluminescent dating using fine grains from pottery. Archaeometry 13, 29–52.

Zubakov, V.A., 1974. Geochronology of the USSR. The Late Pliocene and Quaternary 3. Leningrad: Nedra. 357 pp. in Russian.

Zubakov, V.A., 1988. Climatostratigraphic scheme of the Black Sea Pleistocene and its correlation with the oxygen-isotope scale and glacial events. Quat. Res. 29, 1–24. https://doi.org/10.1016/0033-5894(88)90067-1.